0022-3530/92 $3.00

Petrogenesis of Ultramafic Xenoliths from the 1800 Kaupulehu Flow, Hualalai Volcano, Hawaii

by CHEN-HONG CHEN*, DEAN C. PRESNALL, AND ROBERT J. STERN

Geosciences Program, The University of Texas at Dallas, P.O. Box 830688, Richardson, Texas 75083

(Received 5 August 1987; revised typescript accepted 20 June 1991)

ABSTRACT

The 1800 Kaupulehu flow on Hualalai Volcano, Hawaii, contains abundant xenoliths of dunite, wehrlite, and olivine clinopyroxenite with minor gabbro, troctolite, anorthosite, and websterite. The petrography and mineral compositions of 41 dunite, wehrlite, and olivine clinopyroxenite xenoliths have been studied, and clinopyroxene separates from eight of these have been analyzed for Ba, K, Rb, Sr, rare earth elements, $^{87}Sr/^{86}Sr$, and $^{143}Nd/^{144}Nd$. Temperatures of equilibration obtained by olivine–spinel and pyroxene geothermometry range from 1000 to 1200°C. Mineralogical data combined with published fluid inclusion data indicate depths of origin in the range of 8–30 km.

The rarity of orthopyroxene, the presence of Fe-rich olivine (Fo_{81-89}) and clinopyroxene (Fs_{5-12}), and the occurrence of high TiO_2 in spinel (0·9–2·8 wt.%) and clinopyroxene (0·35–1·33 wt.%) all indicate that the xenoliths are cumulates, not residues from partial fusion. The separated clinopyroxenes have $^{87}Sr/^{86}Sr$ (0·70348–0·70367) and $^{143}Nd/^{144}Nd$ (0·51293–0·51299) values that are different from Sr and Nd isotope ratios of Pacific abyssal basalts (<0·7032 and >0·5130, respectively). Also, clinopyroxenes and spinels in the xenoliths have generally higher TiO_2 contents (>0·35 and >0·91 wt.%, respectively) than their counterparts in abyssal cumulates (<0·40 and <0·70 wt.%, respectively). These differences indicate that the xenoliths are not a normal component of oceanic crust.

Because the xenoliths and alkalic to transitional Hualalai lavas have similar values for $Cr/(Cr+Al)$ and $Cr/(Cr+Al+Fe^{3+})$ of spinels, $^{87}Sr/^{86}Sr$ of clinopyroxenes, and whole-rock $^{3}He/^{4}He$, we conclude that the xenoliths are cumulates from such magmas. Multiple parental magmas for the xenoliths are indicated by slightly heterogeneous $^{87}Sr/^{86}Sr$ of clinopyroxene separates. Depths of formation of the xenoliths are estimated to be ~8–30 km.

Extensive crystallization of olivine in the absence of pyroxenes and plagioclase is a characteristic and prominent feature of Hawaiian tholeiitic magmatism. Dunite xenoliths crystallized from alkalic magmas have previously been reported from Mauna Kea Volcano (Atwill & Garcia, 1985) and Loihi Seamount (Clague, 1988). Our finding of an alkalic signature for dunite xenoliths from a third Hawaiian volcano, Hualalai, shows that early olivine crystallization should be considered a characteristic not just of Hawaiian tholeiitic magmatism but also of Hawaiian alkalic magmatism.

INTRODUCTION

Ultramafic and mafic xenoliths are abundant and well known from the spectacular xenolith cobble beds in the 1800 Kaupulehu alkalic basalt flow on Hualalai Volcano (Richter & Murata, 1961; Jackson, 1968; Bohrson & Clague, 1988). These xenoliths present an excellent opportunity to examine samples of the walls of the conduit through which the magma rose and, thereby, to clarify some aspects of Hawaiian volcanic processes not evident in the lavas themselves. The most abundant xenolith types are dunite, wehrlite, and

* Present address: Institute of Earth Sciences, Academia Sinica, P.O. Box 23–59, Taipei, Taiwan

olivine clinopyroxenite, with gabbro, troctolite, anorthosite, websterite, and two-pyroxene gabbro being much less common. Bohrson & Clague (1988) studied the petrography and mineral compositions of some of the ultramafic xenoliths containing exsolved pyroxenes. Our study complements theirs and concentrates on the abundant dunites, wehrlites, and olivine clinopyroxenites. With one exception, sample 68KAP1, the pyroxenes in the samples of these rocks that we have studied do not show exsolution.

In his pioneering study, White (1966) interpreted ultramafic xenoliths in Hawaiian alkalic basalts to be cumulates from basaltic magma, but he did not specify whether the magma was of Hawaiian or mid-ocean ridge origin. Dunite, wehrlite, and olivine clinopyroxenite xenoliths from Hawaiian alkalic basalts, including those from the 1800 Kaupulehu flow, were interpreted by Jackson (1968) as being partly cumulates and partly texturally deformed restites from partial melting of upper-mantle peridotite. On the basis of a wide and relatively iron-rich range of olivine compositions (Fo_{83-90}), Sen & Presnall (1980, 1986) argued that dunite xenoliths from Koolau Volcano, Oahu, are samples of cumulates from Koolau tholeiites even though the dunite shows deformation textures. Jackson *et al.* (1981) reached a similar conclusion for deformed dunites from the 1800 Kaupulehu flow. However, the similarity of $^3He/^4He$ values ($8 \times$ atmospheric) between Hualalai ultramafic xenoliths and mid-ocean ridge basalts (MORBs) led Kaneoka & Takaoka (1978, 1980), Kyser & Rison (1982), and Rison & Craig (1983) to conclude that these xenoliths are fragments of MORB-type oceanic crust. Dunite and wehrlite xenoliths from Mauna Kea have been interpreted by Atwill & Garcia (1985) as deformed cumulates from Hawaiian alkalic magmas. On the basis of spinel and clinopyroxene compositions, Clague (1988) concluded that dunite and wehrlite xenoliths from Loihi Seamount were crystallized from Hawaiian alkalic magmas.

To clarify the origin of the Kaupulehu ultramafic xenoliths, we have carried out a detailed mineralogical, isotopic, and geochemical study. The petrography and mineral compositions of 46 dunite, wehrlite, and olivine clinopyroxenite xenoliths have been studied. Eight xenoliths were selected for determination of trace element concentrations (REE, K, Rb, Ba, and Sr) and isotopic (Sr and Nd) compositions of separated clinopyroxenes.

SAMPLE LOCATION

The investigated samples were collected from the xenolith beds in olivine-bearing alkalic basalt of the 1800 Kaupulehu flow on the north slope of Hualalai Volcano (Fig. 1). Two outcrops of the uppermost layer of xenoliths were sampled, one located ~ 120 m northeast of the Hue Hue telephone repeater station and the other ~ 120 m southeast of this station (Jackson & Clague, 1981). Samples with the prefixes A, B, and X were collected by the first author. The remainder were supplied by D. A. Clague and B. Melson from the collection of the late E. D. Jackson, now housed at the Smithsonian Institution, Washington, DC.

PETROGRAPHY

The xenoliths typically are subrounded, but some are angular. They have a mean diameter of ~ 7 cm (Jackson *et al.*, 1981). Most consist of varying proportions of olivine, spinel, and clinopyroxene; a few also contain small amounts of plagioclase and orthopyroxene (Table 1). Two main types of xenoliths have been identified, (1) dunite and (2) wehrlite and olivine clinopyroxenite (15–85% clinopyroxene). Several xenoliths are composites of dunite and wehrlite. Two generations of olivine crystals are evident even in hand samples, one comprising large dark crystals and the other made up of smaller and lighter re-

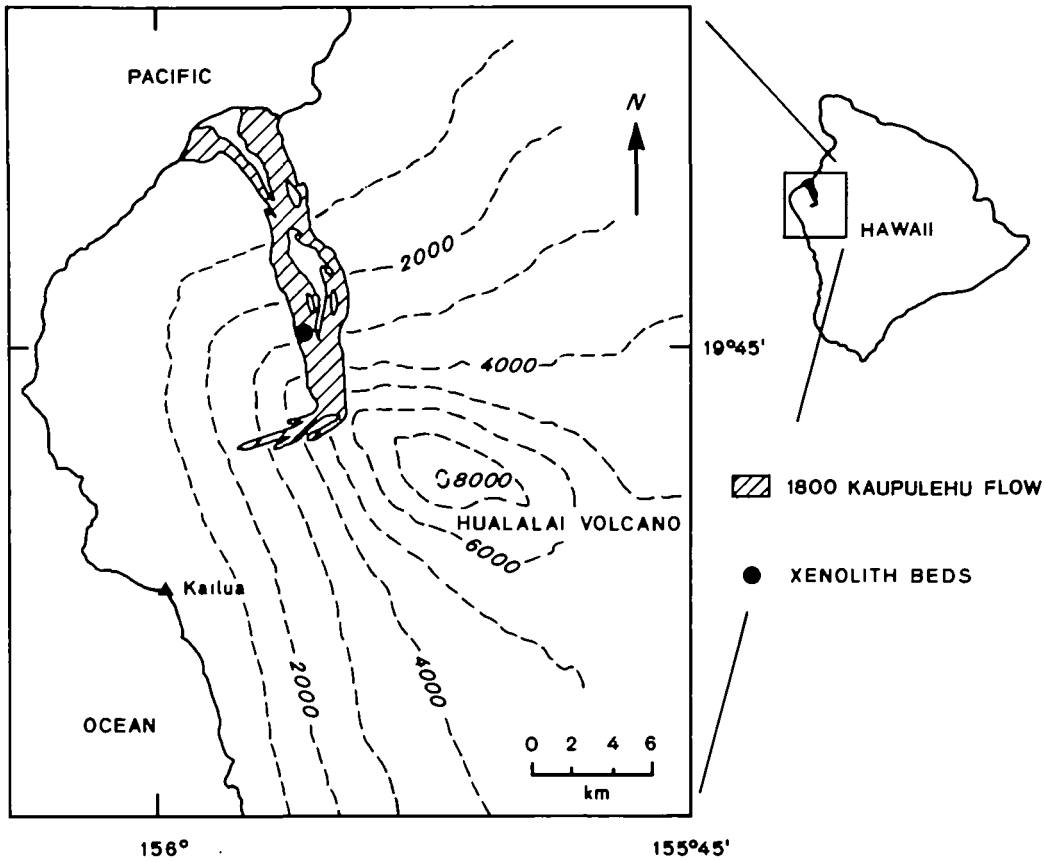

FIG. 1. Map of the island of Hawaii showing the 1800 Kaupulehu alkalic basaltic flow of Hualalai volcano (after Moore *et al.*, 1987) and the site where the xenoliths for this study were collected.

TABLE 1

*Modal percentages of minerals in Kaupulehu xenoliths**

Sample no.	*ol*	*cpx*	*sp*
Dunite			
X2	98	p‡	2
X5A†	99	p	p
X6	99	1	p
X7	95	2	3
X9§	98	2	1
X10	100	p	p
X11§	97	1	2
X12	90	7	3
X14	91	7	3
X21§	97	2	1
X22§	92	4	4
A1	97	2	1
A3§	96	3	1
AA§	92	8	p
B1	98	2	1
B3	91	7	2
B4†§	92	5	3

TABLE 1 (*Continued*)

Sample no.	*ol*	*cpx*	*sp*
65KAP16 (114370/17)‖	97	1	2
66KAP1 (114743/1)‖	98	1	1
68KAP1 (114876/1)†¶	93	4	3
70KAP2 (114970/2)	96	3	1
75KAP5 (115032/1)	94	4	2
75KAP6 (115032/2)	98	—	2
75KAP7 (115032/3)**	96	2	2
75KAP8 (115032/4)	97	1	2
75KAP9 (115032/5)†	98	1	2
Wehrlite and olivine clinopyroxenite			
X1	71	29	—
X3**	26	70	—
X4	40	60	p
X5A†§**	80	15	—
X5§	60	40	—
X8	66	33	2
X17	75	25	1
X20	61	39	p
X23	81	17	2
Q§	30	70	—
B4†§	40	60	—
6511463 (114385/13)§**	40	55	p
65115153 (114386/29)†‖	21	79	—
65KAP17 (114370/18)	57	43	—
66KAP2 (114743/2)§	72	28	—
66KAP3 (114743/3)	15	85	—
68KAP1 (114876/1)†¶**	33	65	—

* Except where indicated, percentages are based on counts of at least 7000 points.

† Composite xenolith.

‡ Present, but <0·5%.

§ From 2500 to 4000 points counted.

‖ Data from Jackson *et al.* (1981).

¶ Cpx has a small amount of exsolved opx. Less than 0·5% opx is present as separate grains in both the dunite and the wehrlite portions.

** Plagioclase present in the following amounts: 75KAP7, <0·5%; X3, 4%; 6511463, 5%; 68KAP1, 1%; X5A, 5% (as a vein).

All samples with the prefixes '65', '66', '68', '70', and '75' are from the collection of E. D. Jackson, housed at the Smithsonian Institution, Washington, DC. They are designated by the numbers assigned by Jackson, with the corresponding Smithsonian numbers in parentheses.

crystallized grains. Examination of thin sections shows that the larger grains commonly contain up to a few volume percent CO_2 and glass inclusions along healed microfractures (see also Kirby & Green, 1980).

Dunite

All the investigated dunite xenoliths are penetratively deformed, and their textures range from porphyroclastic to allotriomorphic granular (Mercier & Nicolas, 1975; Pike &

Schwarzmann, 1977). The most common texture is characterized by kink-banded or strained olivine porphyroclasts (1–5 mm) in a matrix of finer-grained (0·2–0·4 mm) recrystallized, undeformed olivine grains, some of which have rounded to polygonal shapes and well-defined triple junctions. All samples except 75KAP6 contain small amounts of clinopyroxene (augite and subcalcic augite, Table 1). It is pale green in thin section and typically occurs as small ($\sim$30 μm) interstitial grains. Clinopyroxene oikocrysts (up to 1 mm across) with olivine inclusions occur in one sample (X12), whereas clinopyroxene crystals in samples AA, B4, and X4 are blocky and could possibly be cumulus (T. N. Irvine, pers. comm.). Opaque spinel grains of various shapes and sizes (20–400 μm) are ubiquitous. Some occur as small interstitial grains in the fine-grained matrix, some are euhedral or subhedral grains included in olivine, and a few are enclosed in clinopyroxene. The euhedral habit of spinel crystals in olivine indicates that they crystallized relatively early. Orthopyroxene was found only in composite xenolith 68KAP1 and plagioclase was found in one dunite xenolith (75KAP7). Both minerals are interstitial. Inclusions of CO_2 and silicate glass are common along healed microfractures in both clinopyroxene and olivine (Roedder, 1965; Kirby & Green, 1980).

Wehrlite and olivine clinopyroxenite

Three types of clinopyroxene-rich xenoliths were identified by Jackson *et al.* (1981): (1) those that have deformed kink-banded olivine and clinopyroxene in a matrix of recrystallized olivine; (2) those that have kink-banded olivine but undeformed clinopyroxene; and (3) those with undeformed cumulus olivine and intercumulus clinopyroxene. In Table 1, samples X1, X3, X4, X5, X17, X20, X23, Q, B4, 65115153, and 68KAP1 are texture type 1. Samples X5A, X8, and 66KAP2 are texture type 2. Cumulus grain shapes and postcumulus poikilitic textures are common in types 2 and 3. Deformed olivine grains are generally smaller (0·5–1·0 mm) than the porphyroclastic olivine in the dunite xenoliths. Modal mineral proportions for wehrlite and clinopyroxenite xenoliths are given in Table 1. As in the dunite xenoliths, trains of CO_2 and glass inclusions are common in the clinopyroxene and deformed olivine. Rare small interstitial grains of orthopyroxene (only in sample 68KAP1), spinel, and plagioclase also occur.

MINERAL COMPOSITIONS

Olivine

Olivine compositions in the dunite xenoliths range from $Fo_{81\cdot4}$ to $Fo_{89\cdot4}$ (Fig. 2 and Table 2). There is no compositional difference between the large deformed and small recrystallized grains in the same sample. Olivine compositions in wehrlite and olivine clinopyroxenite xenoliths are generally more iron rich ($Fo_{81-84\cdot7}$) than those in the dunites, but the two compositional ranges overlap (Fig. 2 and Tables 2 and 3). NiO contents (0·05–0·28 wt.%) in olivines from wehrlites and clinopyroxenites also overlap those from dunites (0·05–0·50 wt.%). Forsterite content and NiO content of olivine covary.

Spinel

Except in samples X8, X9, X10, and A1, the chemical compositions of spinel grains within a single thin section are identical within analytical uncertainty (Tables 4 and 5). Despite the variations of spinel composition in some samples, a reasonably good positive correlation

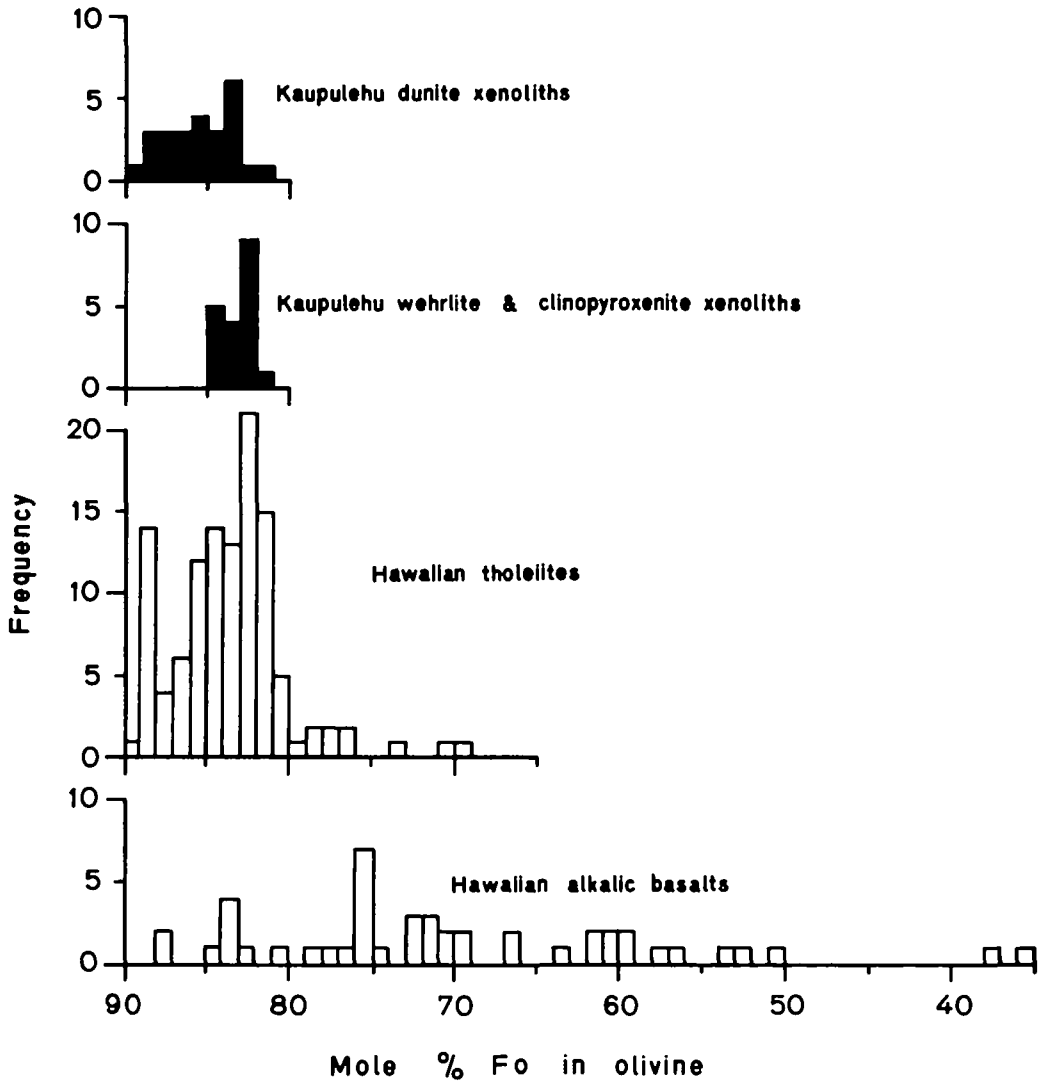

FIG. 2. Histogram of olivine compositions in Hawaiian rocks. Data for Hawaiian tholeiitic and alkalic basalts are from Lofgren *et al.* (1981). Xenolith data are from Tables 2 and 3.

exists between $Mg/(Mg+Fe^{2+})$ in spinel and the forsterite content of coexisting olivine (Tables 2–5), which indicates equilibrium between spinel and coexisting olivine (Sigurdsson, 1977). This correlation is similar to that observed for Mid-Atlantic Ridge basalts (Sigurdsson & Schilling, 1976), for Hawaiian basalts (Evans & Wright, 1972; Clague *et al.*, 1980*a*; Lofgren *et al.*, 1981), and in the Stillwater complex (Jackson, 1969). The only zoned spinel is in sample X2 (Table 5), which shows increasing $Mg/(Mg+Fe^{2+})$ from core to rim.

Clinopyroxene

Within a single thin section, compositions of clinopyroxene grains in the Hualalai ultramafic xenoliths (Tables 6 and 7) are identical within analytical uncertainty. Figure 3

TABLE 2

Olivine compositions in dunite xenoliths (wt.%)

	X2	*X5A*	*X6*	*X7*	*X9*	*X10*	*X11*	*X12*	*X14*	*X21*	*X22*	*A1*	*AA*	*B1*
SiO_2	40·23	39·35	38·47	38·59	39·42	38·74	39·97	39·12	38·84	39·57	39·37	39·20	39·07	39·68
FeO*	12·91	16·10	16·41	14·87	10·84	15·84	11·74	16·01	17·45	10·87	15·42	14·21	15·97	10·45
MgO	46·51	44·58	44·43	45·92	48·81	45·00	48·15	45·11	42·95	48·74	44·85	46·73	45·32	49·49
NiO	0·29	0·18	0·32	0·29	0·48	0·21	0·29	0·19	0·05	0·50	0·30	0·31	0·28	0·37
CaO	0·16	0·27	0·28	0·39	0·19	0·39	0·23	0·29	0·07	—	0·13	0·28	0·29	0·17
Total	100·10	100·48	100·02	99·98	99·74	100·16	100·38	100·72	99·36	99·68	100·07	100·73	100·93	100·16
							Cations per 4 oxygens							
Si	1·000	0·990	0·977	0·973	0·978	0·978	0·987	0·982	0·993	0·981	0·991	0·977	0·979	0·978
Fe	0·268	0·339	0·349	0·313	0·225	0·335	0·242	0·336	0·373	0·225	0·325	0·296	0·335	0·215
Mg	1·723	1·671	1·683	1·725	1·805	1·694	1·772	1·688	1·637	1·802	1·683	1·736	1·693	1·818
Ni	0·006	0·004	0·007	0·006	0·010	0·004	0·006	0·004	0·001	0·010	0·006	0·006	0·006	0·007
Ca	0·004	0·007	0·008	0·011	0·005	0·011	0·006	0·008	0·002	—	0·004	0·007	0·008	0·004
Total	3·000	3·010	3·023	3·027	3·022	3·022	3·013	3·018	3·007	3·019	3·009	3·023	3·021	3·022
% Fo	86·5	83·3	82·8	84·6	88·9	83·5	88·0	83·4	81·4	88·9	83·8	85·4	83·5	89·4

TABLE 2 (*Continued*)

	B3	*B4*	*70KAP2*	*75KAP5*	*75KAP6*	*75KAP7*	*75KAP8*	*75KAP9*	*65115153*	*65KAP16*	*66KAP1*	*68KAP1*
SiO_2	39·46	39·84	40·39	39·57	40·74	39·78	39·93	39·99	39·56	40·57	39·62	39·43
FeO*	13·72	15·11	12·81	12·47	10·97	10·75	13·52	14·15	15·72	12·47	15·28	14·77
MgO	46·74	45·15	46·92	47·71	48·51	47·61	46·29	46·19	45·18	48·09	45·08	45·63
NiO	0·30	0·21	0·28	0·35	0·28	0·36	0·33	0·22	0·28	0·23	—	—
CaO	—	0·26	0·09	0·18	0·14	—	0·18	—	0·21	0·14	—	—
Total	100·22	100·57	100·49	100·28	99·64	100·50	100·25	100·55	100·95	101·50	99·98	99·83
						Cations per 4 oxygens						
Si	0·985	0·996	0·999	0·982	0·998	0·996	0·994	0·994	0·989	0·992	0·995	0·990
Fe	0·286	0·316	0·265	0·259	0·225	0·225	0·282	0·294	0·329	0·255	0·321	0·310
Mg	1·739	1·682	1·730	1·765	1·771	1·776	1·718	1·712	1·683	1·753	1·688	1·709
Ni	0·006	0·004	0·006	0·007	0·006	0·007	0·007	0·004	0·006	0·005	—	—
Ca	—	0·007	0·002	0·005	0·004	—	0·005	—	0·006	0·004	—	—
Total	3·015	3·004	3·001	3·018	3·002	3·004	3·006	3·006	3·011	3·008	3·005	3·010
% Fo	85·9	84·2	86·7	87·2	88·7	87·0	85·9	85·3	83·7	87·3	84·0	84·6

* Total Fe as FeO.

TABLE 3

Olivine compositions in wehrlite and olivine clinopyroxenite xenoliths (wt.%)

	X1	*X3*	*X4*	*X5A*	*X5*	*X8*	*X17*	*X20*	*X23*	*Q*
SiO_2	39·80	38·80	39·70	39·63	39·23	38·78	39·14	38·95	39·06	39·08
FeO*	15·98	18·13	16·45	15·18	16·68	16·27	16·21	16·99	17·09	16·02
MgO	44·31	43·53	44·57	45·80	44·57	44·69	44·53	43·69	44·14	45·19
NiO	0·10	0·20	0·16	0·19	0·18	0·25	—	0·28	0·28	0·25
CaO	—	0·11	—	0·21	0·23	0·28	0·13	—	—	—
Total	100·19	100·77	100·88	101·01	100·89	100·27	100·01	99·91	100·57	100·54
					Cations per 4 oxygens					
Si	1·001	0·983	0·994	0·987	0·985	0·980	0·989	0·989	0·986	0·982
Fe	0·336	0·384	0·345	0·316	0·350	0·344	0·342	0·361	0·361	0·337
Mg	1·661	1·644	1·664	1·700	1·669	1·684	1·677	1·654	1·661	1·693
Ni	0·002	0·004	0·003	0·004	0·004	0·005	—	0·006	0·006	0·005
Ca	—	0·003	—	0·006	0·006	0·008	0·004	—	—	—
Total	2·999	3·017	3·006	3·013	3·015	3·020	3·011	3·011	3·014	3·018
% Fo	83·2	81·1	82·8	84·3	82·6	83·0	83·0	82·1	82·2	83·4

TABLE 3 (*Continued*)

	B4	*66KAP3*	*66KAP2*	*65KAP17*	*65115153*	*6511463*	*68KAP1*	*75KAP9*	*75KAP10*
SiO_2	39·35	39·71	39·85	39·42	39·93	39·30	39·71	39·80	39·72
FeO*	15·19	16·09	14·70	16·36	15·00	16·36	14·71	15·08	16·45
MgO	45·90	44·43	45·68	44·20	45·70	44·19	45·57	45·33	44·07
NiO	0·10	—	—	—	0·17	—	—	—	0·16
CaO	0·19	—	—	—	—	—	—	—	0·20
Total	100·73	100·23	100·23	93·98	100·80	99·85	99·99	100·21	100·60
				Cations per 4 oxygens					
Si	0·983	0·998	0·996	0·995	0·994	0·994	0·995	0·996	0·998
Fe	0·317	0·338	0·307	0·345	0·312	0·346	0·308	0·316	0·346
Mg	1·709	1·665	1·701	1·664	1·696	1·666	1·702	1·692	1·650
Ni	0·002	—	—	—	0·003	—	—	—	0·003
Ca	0·005	—	—	—	—	—	—	—	0·005
Total	3·017	3·002	3·004	3·005	3·006	3·006	3·005	3·004	3·002
% Fo	84·3	83·1	84·7	82·8	83·9	82·8	84·7	84·3	82·7

* Total Fe as FeO.

TABLE 4

Spinel compositions in dunite xenoliths (wt.%)

	X2 (av.)	*X2 (core)*	*X2 (rim)*	*X6*	*X7*	*X9 (1)*	*X9 (2)*	*X10 (1)*	*X10 (2)*	*X11*
SiO_2	0·29	0·35	0·29	0·09	0·11	0·07	0·09	0·05	0·08	0·13
TiO_2	1·67	1·64	1·64	1·72	1·39	1·08	1·36	1·30	1·19	1·30
Al_2O_3	15·28	14·97	14·80	33·40	30·70	27·77	31·75	26·73	34·88	21·93
Cr_2O_3	38·63	38·30	38·79	19·33	25·30	34·43	29·26	25·83	18·33	37·59
FeO*	33·75	32·83	35·70	29·96	28·15	19·50	19·68	31·79	29·30	23·30
MnO	0·25	0·33	0·26	0·15	0·15	0·12	0·15	0·18	0·15	0·19
MgO	9·84	11·10	8·24	14·46	14·36	15·90	16·91	13·30	15·19	14·69
CaO	0·05	—	0·08	—	—	0·04	—	0·11	—	0·02
Total	99·72	99·52	99·80	99·11	99·53	98·91	99·20	99·29	99·12	99·15
Fe_2O_3	13·98	15·19	13·58	14·73	13·32	7·45	8·22	16·52	15·51	10·24
FeO	21·17	19·16	23·48	16·70	16·16	12·80	12·28	16·92	15·34	14·08
New total	101·12	101·04	101·16	100·58	100·86	99·66	100·02	100·94	100·67	100·17
					Cations per 48 oxygens					
Si	0·100	0·120	0·101	0·028	0·035	0·023	0·028	0·016	0·024	0·043
Ti	0·431	0·421	0·428	0·403	0·329	0·257	0·316	0·313	0·276	0·319
Al	6·181	6·021	6·064	12·260	11·157	10·373	11·577	10·120	12·671	8·421
Cr	10·479	10·331	10·657	4·759	6·295	8·625	7·155	6·559	4·465	9·680
Fe^{3+}	3·612	3·900	3·553	3·453	3·155	1·776	1·913	3·995	3·597	2·511
Fe^{2+}	6·075	5·468	6·823	4·348	4·255	3·392	3·177	4·544	3·953	3·837
Mn	0·072	0·096	0·072	0·040	0·040	0·032	0·039	0·049	0·039	0·052
Mg	5·032	5·644	4·268	6·709	6·736	7·508	7·795	6·365	6·975	7·131
Ca	0·019	—	0·029	—	—	0·013	—	0·037	—	0·007
Total	32·001	32·001	31·995	32·000	32·002	31·999	32·000	31·998	32·000	32·001

TABLE 4 (*Continued*)

	X12	*X14*	*X21*	*X22*	*Al (1)*	*Al (2)*	*B1*	*A3*	*B3*	*B4*
SiO_2	0·11	0·32	0·27	0·41	0·08	0·22	—	—	0·20	0·06
TiO_2	1·92	1·15	1·23	0·89	2·57	2·77	1·71	1·25	1·24	1·40
Al_2O_3	29·17	26·91	21·91	31·20	22·38	27·66	29·53	24·73	35·55	26·67
Cr_2O_3	21·97	22·83	38·36	24·74	30·79	25·90	28·92	29·43	21·98	28·24
FeO*	31·73	35·49	21·91	28·89	29·37	28·93	21·91	30·31	25·22	29·49
MnO	0·16	0·17	0·18	0·16	0·18	0·18	0·23	0·20	0·15	0·18
MgO	14·24	12·27	14·85	13·76	13·62	14·59	16·88	13·62	15·63	13·31
CaO	—	0·02	0·02	0·02	—	—	—	—	—	—
Total	99·30	99·16	98·73	100·07	98·99	100·25	99·18	99·54	99·97	99·35
Fe_2O_3	16·74	18·49	9·00	12·84	13·84	13·23	10·86	15·70	11·17	13·76
FeO	16·66	18·85	13·81	17·34	16·91	17·02	12·13	16·18	15·17	17·10
New total	100·97	101·01	99·63	101·36	100·37	101·57	100·26	101·11	101·09	100·72
					Cations per 48 oxygens					
Si	0·035	0·104	0·088	0·128	0·027	0·069	—	—	0·061	0·019
Ti	0·456	0·279	0·303	0·209	0·633	0·657	0·401	0·303	0·284	0·339
Al	10·873	10·245	8·436	11·512	8·637	10·283	10·855	9·407	12·781	10·109
Cr	5·492	5·828	9·904	6·121	7·968	6·456	7·128	7·507	5·299	7·177
Fe^{3+}	3·985	4·495	2·212	3·024	3·411	3·141	2·549	3·813	2·563	3·331
Fe^{2+}	4·405	5·091	3·772	4·537	4·631	4·488	3·164	4·367	3·869	4·599
Mn	0·043	0·047	0·049	0·043	0·049	0·048	0·061	0·055	0·039	0·049
Mg	6·711	5·905	7·288	6·419	6·645	6·856	7·843	6·549	7·104	6·377
Ca	—	0·007	0·007	0·007	—	—	—	—	—	—
Total	32·000	32·001	32·059	32·000	32·001	31·998	32·001	32·001	32·000	32·000

TABLE 4 (*Continued*)

	70KAP2	*75KAP5*	*75KAP6*	*75KAP7*	*75KAP8*	*75KAP9*	*65115153*	*68KAP1*
SiO_2	0·32	0·21	0·33	0·32	0·39	0·33	0·36	—
TiO_2	2·21	1·10	2·09	1·92	1·35	1·49	1·67	1·10
Al_2O_3	24·69	28·73	18·84	23·03	19·67	27·78	25·02	27·55
Cr_2O_3	31·13	29·59	39·47	32·38	36·27	29·97	27·27	28·71
FeO*	26·27	23·29	23·81	27·65	28·92	27·88	32·40	29·32
MnO	0·15	0·14	0·18	0·17	0·18	0·16	0·16	—
MgO	14·24	15·51	14·73	13·86	13·02	13·86	13·48	12·97
CaO	0·11	0·17	0·17	0·10	0·18	0·08	—	—
Total	99·12	98·74	99·62	99·43	99·98	99·55	100·36	99·65
Fe_2O_3	11·17	10·79	10·35	12·51	13·46	12·28	16·43	12·94
FeO	16·21	13·58	14·49	16·39	16·81	16·83	17·61	17·67
New total	100·23	99·82	100·65	100·68	101·33	100·78	102·00	100·94
				Cations per 48 oxygens				
Si	0·104	0·067	0·108	0·104	0·128	0·105	0·115	—
Ti	0·536	0·261	0·516	0·469	0·335	0·357	0·401	0·265
Al	9·396	10·711	7·288	8·816	7·635	10·427	9·440	10·408
Cr	7·944	7·397	10·240	8·312	9·440	7·040	6·899	7·273
Fe^{3+}	2·715	2·569	2·557	3·059	3·335	2·943	3·959	3·121
Fe^{2+}	4·377	3·591	3·977	4·451	4·628	4·481	4·713	4·737
Mn	0·041	0·037	0·051	0·047	0·051	0·043	0·044	—
Mg	6·851	7·309	7·204	6·708	6·388	6·576	6·429	6·195
Ca	0·039	0·057	0·060	0·035	0·064	0·027	—	—
Total	32·003	31·999	32·001	32·001	32·004	31·999	32·000	31·999

* Total Fe as FeO.

For sample X2, (core) and (rim) are individual spot analyses of a single zoned spinel; (av.) is the mean of 15 spot analyses of several spinels including the zoned crystal.

The designations (1) and (2) for samples X9, X10, and Al indicate single spot analyses of two extreme compositions.

TABLE 5

Spinel compositions in wehrlite and olivine clinopyroxenite xenoliths (wt.%)

	X8 (1)	*X8 (2)*	*X17*	*X23*	*75KAP10*
SiO_2	0·08	0·15	0·39	0·27	0·33
TiO_2	1·15	1·41	1·00	0·91	1·84
Al_2O_3	21·40	32·49	27·57	43·42	27·15
Cr_2O_3	32·73	19·54	25·08	10·53	22·90
FeO*	31·69	31·48	32·73	28·47	34·50
MnO	0·17	0·15	0·18	0·13	0·17
MgO	12·19	14·18	12·99	16·07	12·94
CaO	0·05	—	0·05	—	0·15
Total	99·46	99·40	99·99	99·80	99·98
Fe_2O_3	15·43	16·20	16·37	14·35	17·68
FeO	17·80	16·90	17·99	15·55	18·59
New total	101·00	101·02	101·62	101·23	101·75
		Cations per 48 oxygens			
Si	0·027	0·047	0·124	0·080	0·105
Ti	0·285	0·331	0·240	0·203	0·441
Al	8·331	11·952	10·359	15·119	10·215
Cr	8·544	4·820	6·319	2·459	5·777
Fe^{3+}	3·836	3·805	3·928	3·191	4·247
Fe^{2+}	4·915	4·411	4·796	3·843	4·961
Mn	0·040	0·048	0·040	0·032	0·045
Mg	5·999	6·595	6·169	7·075	6·155
Ca	0·017	—	0·017	—	0·051
Total	31·994	32·009	31·992	32·002	31·997

* Total Fe as FeO.

The designations (1) and (2) for sample X8 indicate single spot analyses of two extreme compositions.

shows the range of compositions. These clinopyroxenes are higher in Al_2O_3 and Na_2O (2·5–7·0 and 0·3–1·0 wt.%, respectively) than those from Koolau dunite xenoliths (2·1–2·7 and $<0·4$ wt.%, respectively; Sen & Presnall, 1986), but otherwise they are similar. The Cr_2O_3 and TiO_2 contents are 0·4–1·33 and 0·35–1·3 wt.%, respectively (Table 6 and Fig. 4). Clinopyroxenes in the wehrlite and clinopyroxenite xenoliths are generally higher in iron than those in the dunites (Tables 6 and 7 and Fig. 3), as expected from the analogous difference in the olivine compositions. The clinopyroxenes also show a general decrease in Cr with increasing Fe/Mg.

Orthopyroxene

Apart from its presence as very thin exsolution lamellae in some of the augite grains of sample 68KAP1, the only orthopyroxene observed in the xenoliths occurs as several large (10–15 mm) interstitial grains in both the dunite and the wehrlite parts of composite xenolith 68KAP1. These grains are chemically homogeneous and have higher CaO contents (1·34–1·59 wt.%, Table 8) than orthopyroxene in a dunite xenolith from Koolau Volcano (0·8 wt.%; Sen & Presnall, 1986). This suggests a higher equilibration temperature for the Hualalai sample (Lindsley & Andersen, 1983).

TABLE 6

Clinopyroxene compositions in dunite xenoliths (wt.%)

	X2	*X5A*	*X6*	*X7*	*X9*	*X10*	*X11*	*X12*	*X14*	*X21*	*X22*	*A1*	*A3*
SiO_2	52·78	48·72	49·46	51·11	51·00	51·57	51·99	49·58	50·17	51·65	50·21	49·94	51·40
TiO_2	0·48	1·24	0·82	0·67	0·90	0·51	0·60	0·80	0·67	0·69	0·70	1·14	0·54
Al_2O_3	2·48	7·02	5·41	5·04	4·42	3·47	3·53	5·35	4·85	3·22	5·04	4·60	4·22
Cr_2O_3	0·72	0·40	0·67	0·76	0·67	0·57	1·12	0·74	0·64	1·13	0·88	0·90	0·87
FeO*	3·56	6·43	6·04	5·66	4·00	5·83	4·24	6·04	6·52	3·84	5·46	5·32	5·58
MgO	16·46	15·18	15·69	16·03	17·05	17·02	17·35	16·20	16·01	18·19	15·92	16·54	16·36
CaO	22·77	19·42	21·03	19·94	21·17	20·83	21·10	20·45	20·69	20·89	21·31	20·87	20·84
Na_2O	0·48	0·85	0·59	0·73	0·61	0·32	0·62	0·60	0·58	0·67	0·53	0·65	0·55
Total	99·73	99·26	99·71	99·94	99·82	100·12	100·55	99·76	100·13	100·28	100·05	99·96	100·36
						Cations per 6 oxygens							
Si	1·932	1·806	1·831	1·873	1·866	1·891	1·890	1·832	1·850	1·881	1·847	1·839	1·880
Al^{IV}	0·068	0·194	0·169	0·127	0·135	0·109	0·110	0·168	0·150	0·119	0·153	0·161	0·120
Al^{VI}	0·039	0·113	0·067	0·091	0·056	0·041	0·041	0·065	0·061	0·019	0·066	0·039	0·062
Ti	0·013	0·035	0·023	0·018	0·025	0·014	0·016	0·022	0·019	0·019	0·019	0·032	0·015
Cr	0·021	0·012	0·020	0·022	0·019	0·017	0·032	0·022	0·019	0·033	0·026	0·026	0·025
Mg	0·898	0·839	0·866	0·876	0·930	0·931	0·940	0·892	0·880	0·988	0·873	0·908	0·892
Fe^{2+}	0·109	0·199	0·187	0·173	0·122	0·179	0·129	0·187	0·201	0·117	0·168	0·164	0·171
Ca	0·893	0·771	0·834	0·783	0·830	0·819	0·822	0·810	0·817	0·815	0·840	0·824	0·817
Na	0·034	0·061	0·042	0·052	0·043	0·023	0·044	0·043	0·041	0·047	0·038	0·046	0·039
Total	4·007	4·030	4·039	4·015	4·026	4·024	4·024	4·041	4·038	4·038	4·030	4·039	4·021
mg	89·2	80·8	82·2	83·5	88·4	83·9	87·9	82·7	81·4	89·4	83·9	84·7	83·9
En	47·3	49·2	45·9	47·8	49·4	48·3	49·7	47·2	46·4	51·4	46·4	47·9	47·5
Fs	5·7	10·5	9·9	9·5	6·5	9·3	6·8	9·9	10·6	6·1	8·9	8·6	9·1
Wo	47·0	40·3	44·2	42·7	44·1	42·5	43·5	42·9	43·1	42·5	44·7	43·4	43·5

TABLE 6 (*Continued*)

	AA	*B1*	*B3*	*B4*	*70KAP2*	*75KAP5*	*75KAP6*	*75KAP7*	*75KAP9*	*65115153*	*68KAP1*
SiO_2	50·35	50·72	49·25	51·25	50·88	50·81	52·62	51·40	51·09	51·13	52·00
TiO_2	0·62	1·33	0·98	0·54	0·86	0·74	0·88	0·84	0·67	0·75	0·35
Al_2O_3	5·73	4·52	5·74	3·75	4·17	4·47	3·02	4·26	4·79	4·26	3·91
Cr_2O_3	0·65	1·03	0·92	0·91	0·94	1·07	1·05	1·01	0·96	1·04	0·90
FeO*	6·11	3·81	5·53	5·64	4·73	4·47	4·32	4·83	5·54	5·58	5·78
MgO	16·46	16·30	16·64	16·60	16·92	16·76	17·60	17·23	16·58	15·81	17·40
CaO	19·79	21·10	19·76	20·52	20·60	21·25	20·60	19·85	19·30	21·71	18·99
Na_2O	0·52	0·93	0·88	0·50	0·73	0·58	0·61	0·84	1·00	0·55	0·69
Total	100·23	99·74	99·70	99·71	99·83	100·15	100·70	100·26	99·93	100·02	100·83
					Cations per 6 oxygens						
Si	1·843	1·860	1·817	1·887	1·867	1·859	1·906	1·874	1·871	1·869	1·898
Al^{IV}	0·156	0·140	0·184	0·113	0·132	0·141	0·094	0·126	0·129	0·132	0·101
Al^{VI}	0·091	0·055	0·066	0·050	0·048	0·052	0·035	0·057	0·078	0·052	0·067
Ti	0·017	0·037	0·027	0·015	0·024	0·020	0·024	0·023	0·018	0·021	0·010
Cr	0·019	0·030	0·027	0·026	0·027	0·031	0·030	0·029	0·028	0·030	0·026
Mg	0·898	0·891	0·915	0·911	0·926	0·914	0·950	0·936	0·905	0·861	0·947
Fe^{2+}	0·187	0·117	0·171	0·174	0·145	0·137	0·131	0·147	0·170	0·171	0·177
Ca	0·776	0·829	0·781	0·810	0·810	0·833	0·799	0·775	0·758	0·850	0·743
Na	0·037	0·066	0·063	0·036	0·052	0·041	0·043	0·059	0·071	0·039	0·049
Total	4·026	4·025	4·051	4·022	4·031	4·028	4·012	4·026	4·028	4·025	4·018
mg	82·8	88·4	84·3	84·0	86·4	87·0	87·9	86·4	84·2	83·5	84·3
En	48·3	48·5	49·0	48·1	49·2	48·5	50·5	50·4	49·4	45·8	50·7
Fs	10·0	6·4	9·1	9·2	7·7	7·3	7·0	7·9	9·3	9·1	9·5
Wo	41·7	45·1	41·8	42·7	43·1	44·2	42·5	41·7	41·3	45·2	39·8

* Total Fe as FeO.

TABLE 7

Clinopyroxene compositions in wehrlite and olivine clinopyroxenite xenoliths (wt.%)

	X1	*X3*	*X4*	*X5A*	*X5*	*X8*	*X17*	*X20*	*X23*	*Q*
SiO_2	50·93	49·91	51·01	52·21	51·81	51·94	50·30	50·65	49·59	50·46
TiO_2	0·50	0·79	0·58	0·48	0·57	0·55	0·73	0·60	0·78	0·60
Al_2O_3	4·56	5·63	4·67	3·64	4·17	4·48	5·03	5·51	6·56	5·16
Cr_2O_3	0·56	0·41	0·50	0·52	0·52	0·60	0·71	0·37	0·40	0·63
FeO*	6·03	7·26	6·30	5·23	6·45	6·30	6·11	7·01	7·00	6·12
MgO	16·44	15·93	16·56	17·61	16·86	16·08	15·78	16·67	15·23	16·51
CaO	21·17	19·76	20·17	19·45	19·23	19·54	20·80	18·79	19·97	19·96
Na_2O	0·39	0·58	0·44	0·51	0·60	0·58	0·58	0·55	0·71	0·51
Total	100·58	100·27	100·23	99·65	100·21	100·07	100·04	100·15	100·24	99·95
					Cations per 6 oxygens					
Si	1·864	1·837	1·869	1·908	1·893	1·899	1·852	1·856	1·825	1·854
Al^{IV}	0·136	0·163	0·131	0·092	0·107	0·101	0·147	0·144	0·176	0·147
Al^{VI}	0·061	0·081	0·071	0·065	0·073	0·092	0·071	0·094	0·109	0·077
Ti	0·014	0·022	0·016	0·013	0·016	0·015	0·020	0·017	0·022	0·017
Cr	0·016	0·012	0·014	0·015	0·015	0·015	0·017	0·021	0·011	0·012
Mg	0·897	0·874	0·905	0·959	0·918	0·877	0·866	0·910	0·835	0·904
Fe^{2+}	0·185	0·223	0·193	0·160	0·197	0·193	0·188	0·215	0·215	0·188
Ca	0·830	0·779	0·792	0·762	0·753	0·766	0·821	0·738	0·787	0·786
Na	0·028	0·041	0·031	0·036	0·043	0·041	0·041	0·039	0·051	0·036
Total	4·031	4·032	4·022	4·010	4·015	3·999	4·023	4·034	4·031	4·021
mg	82·9	79·6	82·4	85·7	82·3	82·0	82·2	80·9	79·5	82·8
En	46·9	46·6	47·9	51·0	49·2	47·8	46·2	48·9	45·4	48·1
Fs	9·7	11·9	10·2	8·5	10·5	10·5	10·0	11·5	11·7	10·0
Wo	43·4	41·5	41·9	40·5	40·3	41·7	43·8	39·6	42·8	41·8

TABLE 7 (*Continued*)

	B4	*66KAP3*	*66KAP2*	*65KAP17*	*6511463*	*65115153*	*68KAP1*	*75KAP9*	*75KAP10*
SiO_2	51·29	50·88	50·80	49·55	49·37	51·21	51·00	51·41	50·19
TiO_2	0·57	0·50	0·56	0·67	0·65	0·62	0·50	0·46	0·72
Al_2O_3	3·46	4·40	4·93	5·78	5·34	4·17	4·74	4·64	5·16
Cr_2O_3	0·95	0·39	0·82	0·52	0·61	0·69	0·72	1·02	0·60
FeO*	5·60	5·93	5·60	6·13	5·89	5·59	6·05	5·88	6·33
MgO	17·26	17·58	16·50	15·89	16·24	16·38	17·28	17·28	15·96
CaO	20·49	19·32	20·74	20·96	21·80	21·10	19·08	18·43	20·71
Na_2O	0·49	0·56	0·41	0·51	0·43	0·40	0·70	0·79	0·52
Total	100·11	99·56	100·36	100·01	100·33	100·16	100·07	99·91	100·09
				Cations per 6 oxygens					
Si	1·882	1·871	1·858	1·827	1·820	1·878	1·867	1·880	1·847
Al^{IV}	0·118	0·129	0·142	0·173	0·180	0·122	0·133	0·121	0·154
Al^{VI}	0·032	0·062	0·071	0·078	0·052	0·058	0·071	0·079	0·070
Ti	0·016	0·014	0·015	0·019	0·018	0·017	0·014	0·013	0·020
Cr	0·028	0·011	0·024	0·015	0·018	0·020	0·021	0·029	0·017
Mg	0·944	0·964	0·900	0·873	0·892	0·895	0·943	0·942	0·875
Fe^{2+}	0·172	0·182	0·171	0·189	0·182	0·171	0·185	0·180	0·195
Ca	0·806	0·761	0·813	0·828	0·861	0·829	0·749	0·722	0·816
Na	0·035	0·040	0·029	0·036	0·031	0·028	0·050	0·056	0·037
Total	4·033	4·034	4·023	4·038	4·054	4·018	4·033	4·022	4·031
mg	84·6	84·1	84·0	82·2	83·1	83·9	83·6	84·0	81·8
En	49·1	50·5	47·8	46·2	46·1	47·2	50·4	51·1	46·4
Fs	8·9	9·6	9·1	10·0	9·4	9·0	9·8	9·8	10·3
Wo	41·9	39·9	43·1	43·8	44·5	43·7	39·9	39·2	43·3

* Total Fe as FeO.

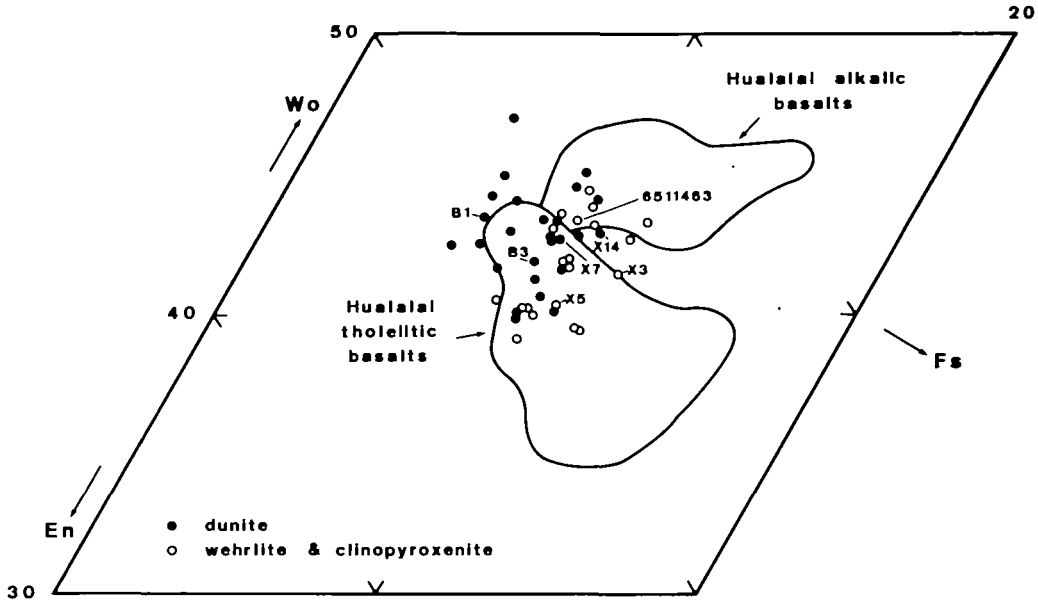

FIG. 3. Clinopyroxene compositions for Hualalai lavas and Kaupulehu xenoliths plotted in the $CaSiO_3$(wo)–$MgSiO_3$(en)–$FeSiO_3$(fs) triangle (mole percent). Clinopyroxene samples analyzed for trace elements are labeled. Hualalai tholeiitic and alkalic basalt fields are from Bohrson & Clague (1988).

TRACE ELEMENT AND ISOTOPIC COMPOSITIONS OF CLINOPYROXENES

Isotopic analyses for Sr and Nd and the concentrations of K, Rb, Sr, Ba, and rare earth elements (REE), in the clinopyroxene separates from four dunite, two wehrlite, and two olivine clinopyroxenite samples are given in Table 9 (see Appendices A and B for analytical methods). All the separates were acid leached after careful hand-picking to remove possible surface contaminants. The investigated samples were chosen to cover the entire range of Mg/Fe for clinopyroxene in the Hualalai xenoliths (Tables 6 and 7). Except for dunite sample X14, REE concentrations of clinopyroxene in the dunite xenoliths are higher than those in clinopyroxene from wehrlite and clinopyroxenite xenoliths (Table 9 and Fig. 5). All eight REE patterns are convex upward (Fig. 5). Except for Sr, the concentrations of other trace elements (K, Rb, Ba), are very low (Table 9). The clinopyroxene separates have $^{143}Nd/^{144}Nd$ ranging from 0·51293 to 0·51299 and $^{87}Sr/^{86}Sr$ ranging from 0·70348 to 0·70367.

EQUILIBRATION TEMPERATURES

Because of the very limited occurrence of orthopyroxene, geothermometry based on an assumption of coexisting pyroxenes must rely entirely on clinopyroxene compositions, and therefore it yields only minimum temperatures. The method of Lindsley & Andersen (1983) gives values from 1000 to 1220 °C. On average, they are ~55 °C higher than values determined by the method of Kretz (1982) and about 130 °C higher than those calculated by the procedure of Mysen (1976). One exceptional xenolith, dunite sample X2, has a relatively low Lindsley–Anderson temperature of 915 °C. Sample 68KAP1, the only sample with coexisting clinopyroxene and orthopyroxene, has a Lindsley–Andersen temperature of

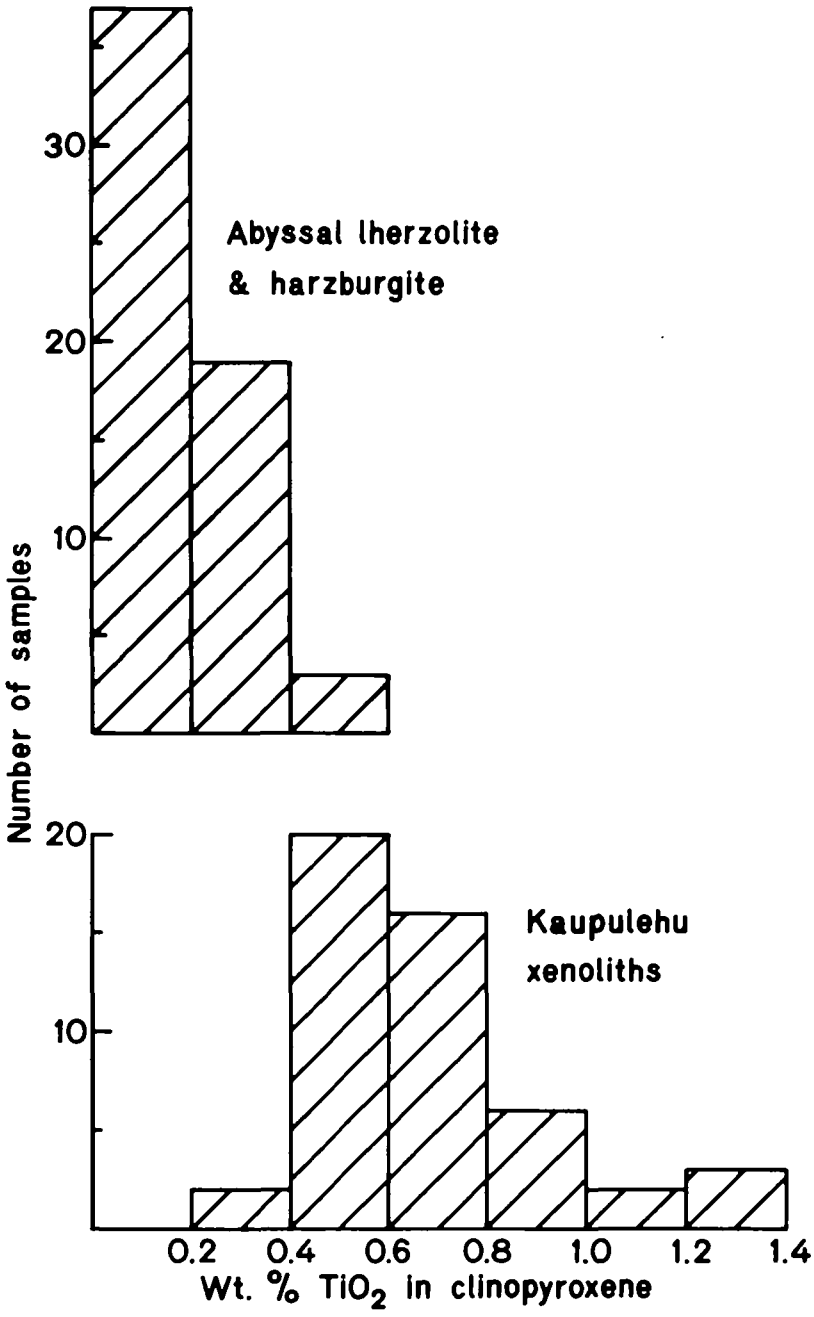

FIG. 4. Histogram of wt.% TiO_2 in clinopyroxenes. Hualalai xenolith data are from Tables 6 and 7. Abyssal peridotite data are from Clarke & Loubat (1977), Arai & Fujii (1979), Hamlyn & Bonatti (1980), Hebert *et al.* (1983), Dick & Bullen (1984), and Dick (1989).

1185 °C and a Kretz temperature of 1166 °C, in good accord with values for the other ultramafic xenoliths in which orthopyroxene is absent.

Four olivine–spinel thermometers were tried. They give temperatures that are, on average, higher than those given by the Lindsley–Andersen pyroxene thermometer by 13 °C

TABLE 8

Orthopyroxene compositions (wt.%) in composite xenolith 68KAP1

	Wehrlite	*Dunite*
SiO_2	52·95	54·78
TiO_2	0·31	0·21
Al_2O_3	4·91	3·43
Cr_2O_3	0·25	0·33
FeO*	10·13	9·87
MgO	30·02	30·40
CaO	1·59	1·34
Na_2O	0·13	0·11
Total	100·29	100·47
	Cations per 6 oxygens	
Si	1·864	1·917
Al^{IV}	0·136	0·083
Al^{VI}	0·086	0·059
Ti	0·008	0·006
Cr	0·007	0·009
Mg	1·576	1·586
Fe	0·298	0·289
Ca	0·060	0·050
Na	0·009	0·007
Total	4·026	4·006
mg†	84·1	84·6
En	81·5	82·4
Fs	15·4	15·0
Wo	3·1	2·6

* Total Fe as FeO.
† $mg = Mg \times 100/(Mg + Fe)$.

(Roeder *et al.*, 1979), 73 °C (Fujii, 1978, with $\ln k = 2$), 90 °C (Fabries, 1979), and 145 °C (Engi, 1983, CO type diagram). Because the pyroxene temperatures are minimum values, the slightly higher olivine–spinel temperatures (except possibly the extremely high values obtained by the Engi procedure) are considered to be generally consistent with the pyroxene temperatures. The large scatter of temperatures determined by the various thermometers precludes all but the simplest conclusion that the temperatures are in or only slightly below the magmatic range, a conclusion consistent with the general lack of pyroxene exsolution. This interpretation implies that the observed deformation and recrystallization, especially in the dunites, occurred at temperatures only slightly below the solidus.

DEPTH OF FORMATION

Roedder (1965) found a minimum depth for trapping of CO_2 inclusions in olivine from Hualalai dunites of 8–15 km (Roedder, 1965). The association of olivine, plagioclase, orthopyroxene, and clinopyroxene in one Hualalai ultramafic xenolith (68KAP1, Table 1) indicates a maximum depth of formation of ~30 km, the maximum depth for stability of plagioclase lherzolite (Green & Hibberson, 1976; Presnall *et al.*, 1979). These limits of ~8–30 km correspond to lower-crust to uppermost-mantle depths in Hawaii. Because most of the xenoliths do not have plagioclase, the maximum depth must be considered to be tentative.

TABLE 9

Trace element concentrations and isotope ratios of clinopyroxene separates

	Dunite				*Wehrlite*		*Clinopyroxenite*	
	B1	*B3*	*X7*	*X14*	*Q*	*6511463*	*X3*	*X5*
REE (ppm)								
Ce	30·31	12·63	8·91	5·11	3·62	4·81	3·93	3·50
Nd	32·81	9·53	6·67	5·11	3·75	4·86	4·39	3·07
Sm	10·51	2·72	2·05	1·70	1·31	1·68	1·63	1·08
Eu	3·15	0·96	0·73	0·61	0·49	0·57	0·64	0·39
Gd	9·44	2·90	2·22	2·12	1·69	1·88	2·17	1·32
Dy	9·62	3·32	2·29	2·04	1·66	1·81	2·19	1·29
Er	4·47	1·63	1·14	0·95	0·79	0·81	1·04	0·60
Yb	2·85	1·32	0·86	0·71	0·61	0·62	0·81	0·44
K (ppm)	27·2	15·3	15·7	17·7	49·8	26·8	24·1	36·7
Rb	0·12	0·10	0·04	0·04	0·16	0·08	0·07	0·13
Ba	1·8	1·1	0·6	0·6	1·7	0·9	1·6	1·2
Sr	71·9	84·4	74·6	39·1	43·4	37·6	45·1	40·3
$^{87}Sr/^{86}Sr$	0·70361 ±9	0·70353 ±5	0·70348 ±7	0·70351 ±6	0·70357 ±6	0·70360 ±3	0·70367 ±5	0·70351 ±8
$^{143}Nd/^{144}Nd$	0·512931 ±21	0·512985 ±17	0·512933 ±20	0·512945 ±38	0·512972 ±20	0·512965 ±23	0·512963 ±24	0·512946 ±17
% Fo (ol)	89·4	85·9	84·6	81·4	83·4	83·1	81·1	82·6
mg (cpx)	88·4	84·3	83·5	81·4	82·8	82·8	79·6	82·3
% Na_2O (cpx)	0·93	0·88	0·73	0·58	0·51	0·43	0·58	0·60

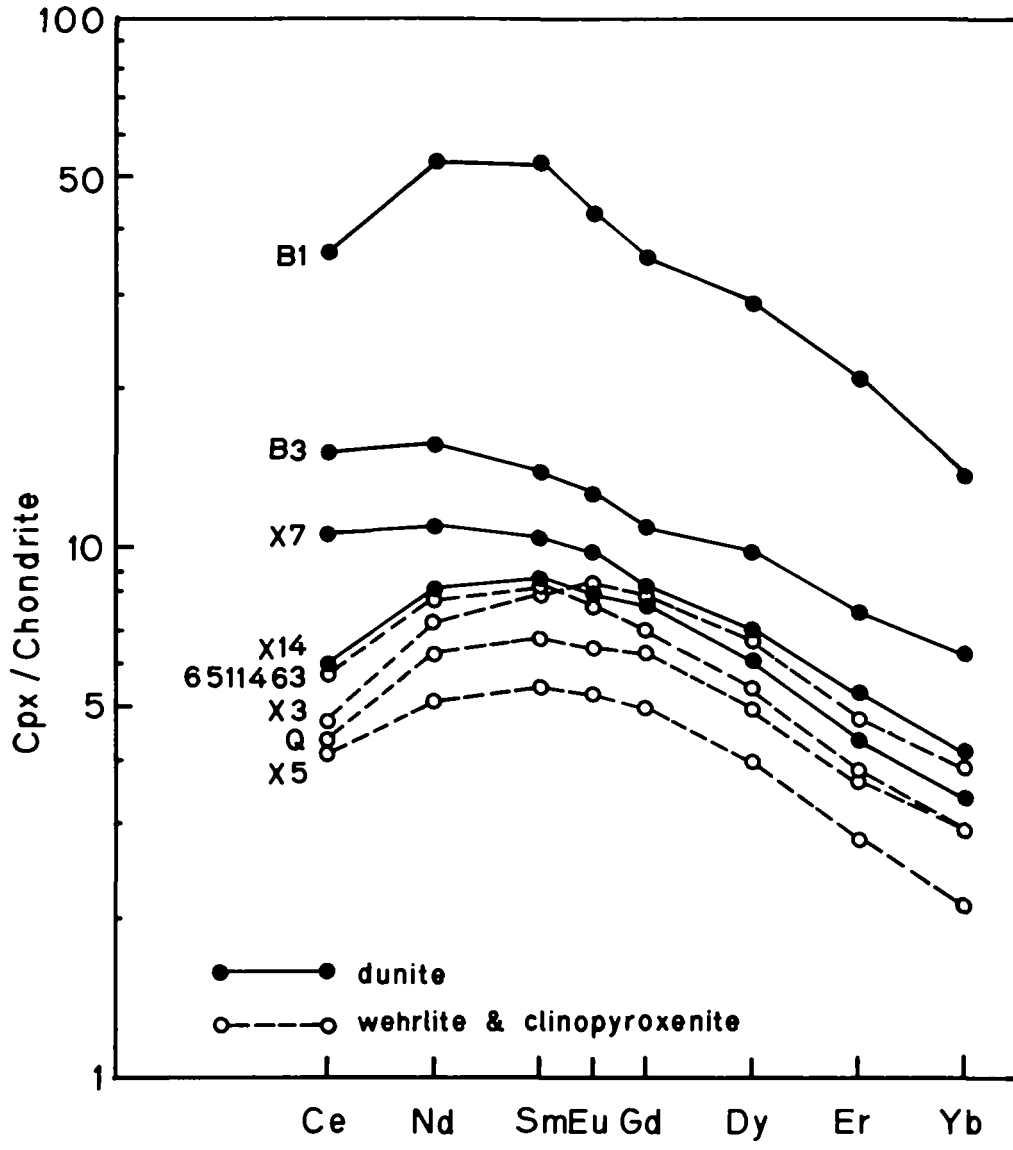

FIG. 5. Chondrite-normalized REE patterns for clinopyroxenes from dunite, clinopyroxenite, and wehrlite xenoliths in the Kaupulehu flow. Data are from Table 9.

ORIGIN OF HUALALAI ULTRAMAFIC XENOLITHS

In discussing the origin of the Hualalai ultramafic xenoliths, we first consider whether the xenoliths are restites from partial melting of upper-mantle peridotite or cumulates formed by fractional crystallization of basaltic magma. We then consider whether the basaltic magma was associated with Hawaiian volcanism or had oceanic crustal (MORB) affinities. Finally, for the case of a Hawaiian affinity, we consider whether the parental magmas were alkalic or tholeiitic.

Residues of partial fusion

Olivine from abyssal peridotites has a higher and narrower range of forsterite content ($Fo_{89\cdot3-91\cdot6}$) than olivine from the Kaupulehu ultramafic xenoliths (Prinz *et al.*, 1976; Sinton, 1979; Hebert *et al.*, 1983; Dick & Fisher, 1984; Dick, 1989). A peridotite from Zabargad Island in the Red Sea, which has been proposed as a sample of undepleted oceanic mantle (Bonatti *et al.*, 1986), shows an olivine composition range of $Fo_{87\cdot3-90\cdot5}$. The pyrolite model mantle composition of Ringwood (1975) has an olivine composition of Fo_{90}, and Carter (1970) proposed that olivines from undepleted upper mantle beneath Kilbourne Hole, New Mexico, has compositions of Fo_{86-88}. Thus, olivine in both depleted and undepleted upper-mantle peridotite is more Mg rich than most of the olivine in the Kaupulehu ultramafic xenoliths. These differences are inconsistent with a mantle residue origin for the Kaupulehu dunites and wehrlites.

A similar argument can be made on the basis of the pyroxene compositions. Most clinopyroxene from abyssal peridotites has a higher and narrower range of 100Mg/(Mg + Fe) (89·5–92·8, Prinz *et al.*, 1976; Symes *et al.*, 1977; Arai & Fujii, 1979; Sinton, 1979; Hamlyn & Bonatti, 1980; Hebert *et al.*, 1983; Dick & Fisher, 1984; Dick, 1989), than that of clinopyroxene from Kaupulehu ultramafic xenoliths (80·8–89·2, Table 7). Orthopyroxene from abyssal peridotites is normally more magnesian than En_{86} (Prinz *et al.*, 1976; Symes *et al.*, 1977; Arai & Fujii, 1979; Sinton, 1979; Hamlyn & Bonatti, 1980; Hebert *et al.*, 1983; Dick & Fisher, 1984; Dick, 1989), whereas the one orthopyroxene composition we have determined from a Kaupulehu xenolith is En_{82} (Table 6). These differences argue against a mantle residue origin.

Figure 4 shows that the range of TiO_2 content of clinopyroxene in abyssal peridotites is very low (<0·5 wt.%) and easily distinguished from that of clinopyroxene in Hualalai ultramafic xenoliths. Also, the $Fe^{3+}/(Fe^{3+} + Cr + Al)$ values of spinel in Hualalai xenoliths (0·09–0·21) are generally higher than those of spinel in abyssal peridotites (usually <0·1, see Prinz *et al.*, 1976; Sinton, 1979; Hebert *et al.*, 1983; Dick & Bullen, 1984; Dick, 1989). The amounts of TiO_2 in spinel from abyssal peridotites are <0·8 wt.% (Arai & Fujii, 1977; Clarke & Loubat, 1977; Hamlyn & Bonatti, 1980; Hebert *et al.*, 1983; Dick & Bullen, 1984; Dick, 1989), which is low compared with the TiO_2 contents of spinel from the Hualalai ultramafic xenoliths (0·9–2·8 wt.%). Because abyssal peridotites are generally considered to be restites from partial fusion (Dick & Bullen, 1984; Dick, 1989), these data also support the conclusion that the Hualalai ultramafic xenoliths were not produced by partial melting of upper-mantle peridotite.

Finally, we argue on the basis of phase relationships that the xenoliths are not residues from partial fusion. The first liquid produced on melting a spinel lherzolite would drive the residue toward the olivine–orthopyroxene join (Takahashi & Kushiro, 1983; Presnall & Hoover, 1987). With continued melting, the residue would change from lherzolite (ol + opx + cpx + sp) to harzburgite (ol + opx), and finally to dunite. Lherzolite and harzburgite are not found as xenoliths in the Kaupulehu flow. The common occurrence of clinopyroxene, coupled with the complete absence of orthopyroxene from all but one xenolith, is incompatible with a mantle residue origin.

Cumulates formed as a part of the oceanic crust

On the basis of (1) the occurrence of cumulate textures in the clinopyroxene-rich xenoliths, and (2) the generally greater Fe/Mg enrichment of the wehrlites and clinopyroxenites relative to the dunites, we conclude that the Kaupulehu ultramafic xenoliths are

cumulates formed by crystallization of olivine and then clinopyroxene + olivine from a fractionating magma. Evidence will be presented below that the xenoliths were not all crystallized from the same magma, but this complication would not significantly disturb the overall differences in Fe/Mg between rock types as long as the different parental magmas were compositionally similar.

A further question concerns the MORB or Hawaiian affinity of the magmas from which the Kaupulehu cumulates crystallized. Bohrson & Clague (1988) have pointed out that the TiO_2 content of spinels in Kaupulehu xenoliths that they studied is generally higher than typical values (<1%) for spinels crystallized from MORBs. They used this difference to argue that the xenoliths did not crystallize from MORBs. Our results (Tables 4 and 5) are consistent with theirs. Furthermore, if the clinopyroxene in the pyroxenite and wehrlite xenoliths is cumulus, as argued below, the concentration of Sr in the coexisting liquids would be 313–703 ppm (using $D_{Sr}=0{\cdot}12$; Arth, 1976). This is distinct from the average of 127 ppm (Lofgren *et al.*, 1981) and 80–145 ppm (Sun *et al.*, 1979) reported for MORBs.

Pacific MORBs have low $^{87}Sr/^{86}Sr$ (<0·7032) and high $^{143}Nd/^{144}Nd$ (>0·5130) (Fig. 6). Strontium and Nd isotopic ratios of clinopyroxene in the Kaupulehu ultramafic xenoliths are distinct from those of East Pacific Rise basalts but are similar to those of other Hawaiian basalts (Fig. 6). Therefore, a Hawaiian parentage for the ultramafic xenoliths is indicated. Clinopyroxene in two unusual gabbroic xenoliths from the Kaupulehu flow has lower $^{87}Sr/^{86}Sr$ (0·70285 ± 6) and higher $^{143}Nd/^{144}Nd$ (0·51317 ± 2) values (Clague & Chen, 1986) than those of the ultramafic xenoliths. These two gabbroic xenoliths are distinct from other gabbroic xenoliths in the Kaupulehu flow and were interpreted by Clague & Chen as rare fragments of oceanic crust entrapped in this flow with other xenoliths of Hawaiian origin.

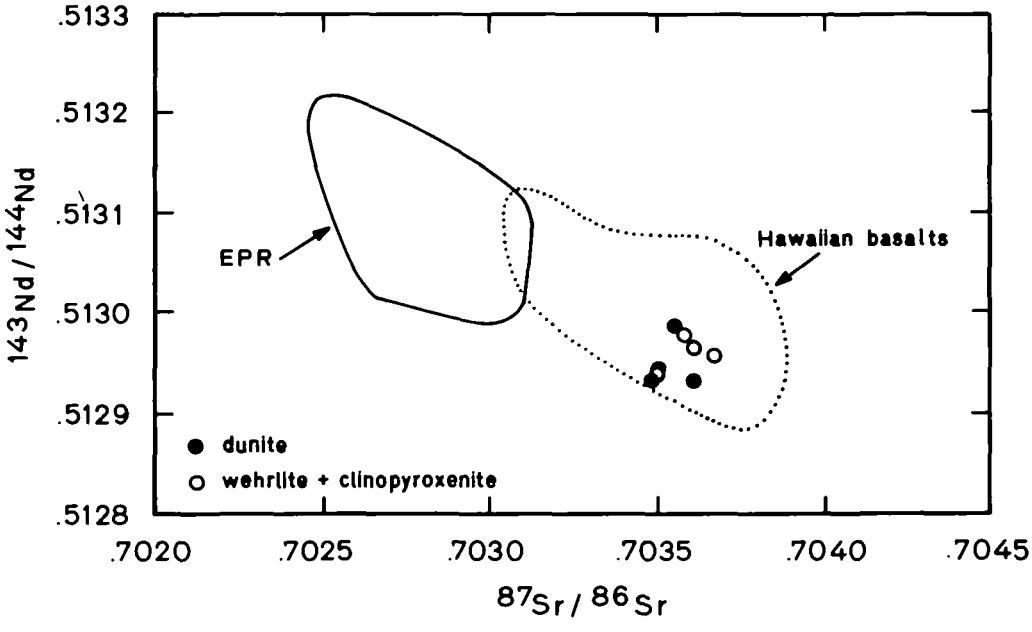

FIG. 6. Comparison of Nd and Sr isotopic compositions for Kaupulehu xenoliths with those of basalts from Hawaii and the East Pacific Rise (EPR). The fields for lavas are from Staudigel *et al.* (1984), Roden *et al.* (1984), and Chen & Frey (1985).

Kaneoka & Takaoka (1980), Kyser & Rison (1982), and Rison & Craig (1983) have argued, on the basis of similar $^3He/^4He$ values, that the Hualalai xenoliths are fragments of normal oceanic crust. However, a very wide range of $^3He/^4He$ values [(6·6–32) × atmospheric] is found in Hawaiian basalts (Kaneoka & Takaoka, 1980; Kyser & Rison, 1982; Kurz *et al.*, 1983, 1987, 1990; Rison & Craig, 1983; Lupton & Garcia, 1986), and many Hawaiian alkalic basalts have $^3He/^4He$ values similar to those of MORBs. These data indicate that similarities of $^3He/^4He$ between Hualalai ultramafic xenoliths and MORB are not diagnostic of a normal oceanic crustal origin.

We conclude, on the basis of TiO_2 content of the spinels, calculated Sr concentrations of coexisting liquids, and Nd and Sr isotopic data, that the Hualalai ultramafic xenoliths are not fragments of oceanic crustal material produced at a spreading center.

Cumulates from Hualalai magmas

The only remaining explanation for the origin of the Hualalai ultramafic xenoliths is that they are cumulates crystallized from Hawaiian magmas. Because the vent for the Kaupulehu flow lies at least 25 km from any of the rifts extending from the summit areas of adjacent Hawaiian volcanoes, the magmas from which the xenoliths crystallized are almost certainly Hualalai magmas. Hualalai has produced both tholeiitic and alkalic lavas, so a further question concerns the type of magma involved. Bohrson & Clague (1988) concluded that the xenoliths in the Kaupulehu flow were crystallized from tholeiitic magmas, and Sen & Presnall (1986) reached a similar conclusion for dunite xenoliths from Koolau volcano on Oahu. In this section we use major element, trace element, and isotopic data along with mineralogical and phase equilibrium relationships to re-examine this issue for the xenoliths in the Kaupulehu flow.

Major element data

Figures 7 and 8 show that spinels in Koolau dunite xenoliths have generally high Cr/(Cr + Al) ratios like those in Hualalai tholeiites but widely varying $Fe^{3+}/(Cr + Al + Fe^{3+})$ like those in Hualalai alkalic basalts. Evidently, comparisons between different volcanoes can yield inconsistent results. In any case, the complete separation of the Koolau spinel composition field from that of spinels from xenoliths in the Kaupulehu flow suggests a different origin for the two suites.

Fodor *et al.* (1975) and Lofgren *et al.* (1981) have shown that clinopyroxenes in Hawaiian tholeiitic basalts have lower normative wollastonite (Wo) content than those from Hawaiian alkalic basalts, and Bohrson & Clague (1988) have confirmed this relationship for Hualalai lavas. As shown in Fig. 3, clinopyroxene compositions in the xenoliths range across both the tholeiitic and alkalic clinopyroxene fields for Hualalai lavas, and in some cases lie outside both fields. Lavas elsewhere in Hawaii show somewhat larger clinopyroxene composition fields. An especially well-documented case is the transitional to alkalic East Molokai stratigraphic section studied by Beeson (1976). He showed (see his fig. 21) that clinopyroxenes in the stratigraphically highest and most strongly alkalic lavas have a minimum $CaSiO_3$ proportion of ~41%, which decreases down-section to ~35% just above the tholeiitic lavas. The minimum $CaSiO_3$ percentage we find for clinopyroxenes in the Hualalai xenoliths is ~39%. Thus, comparison with the East Molokai lavas leads to the conclusion that the parental magmas for the xenoliths were alkalic to transitional. The data from East Molokai suggest that the fields for clinopyroxenes from Hualalai lavas may be unrealistically small because of a limited sample size.

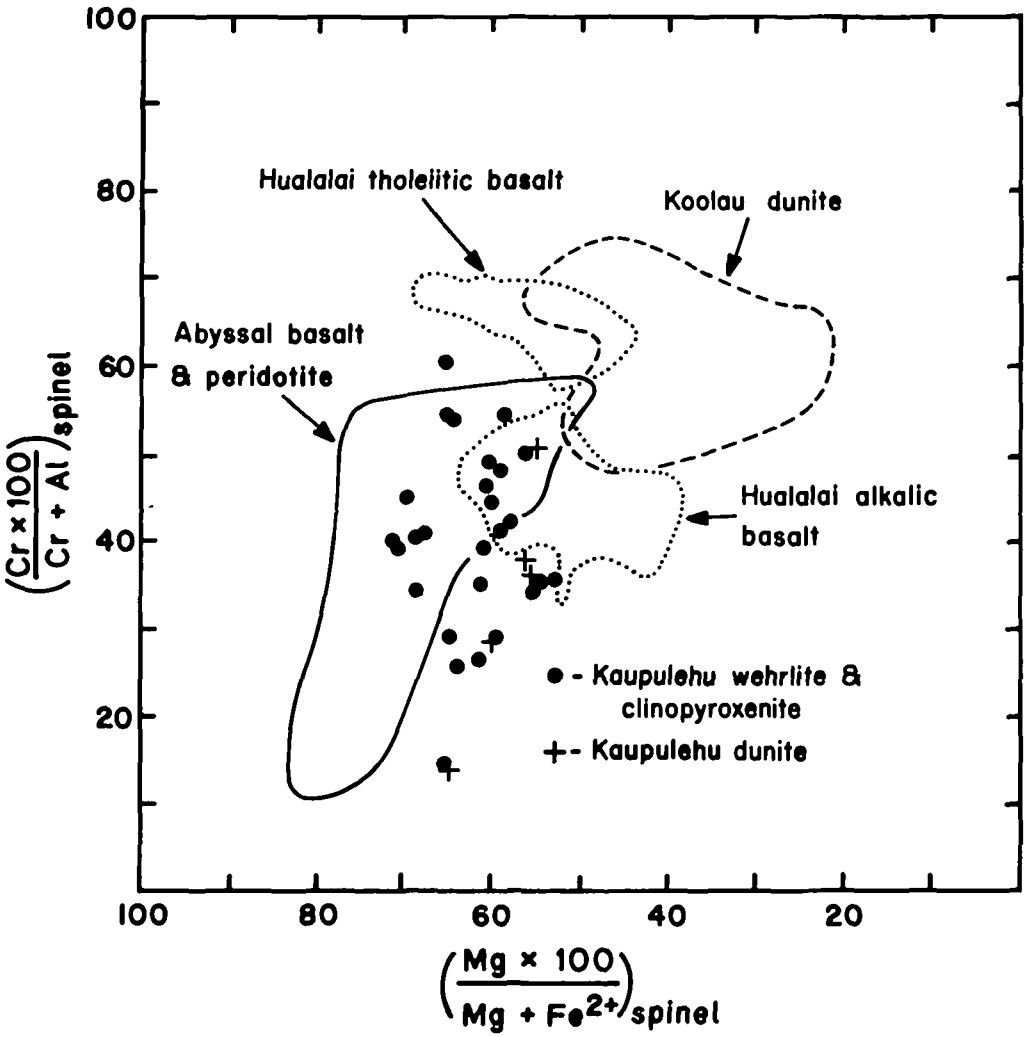

FIG. 7. Comparison of spinel compositions (cation ratios) in Kaupulehu ultramafic xenoliths (data from Tables 4 and 5) with those in Hualalai alkalic and tholeiitic basalts (data from Bohrson & Clague, 1988), Koolau dunite xenoliths (data from Sen & Presnall, 1986), and abyssal basalt and peridotite (data from Clarke & Loubat, 1977; Arai & Fujii, 1979; Hamlyn & Bonatti, 1980; O'Donnell & Presnall, 1980; Hebert *et al.*, 1983; Dick & Bullen, 1984; Dick, 1989).

Rare earth element data

Use of clinopyroxene rare earth element (REE) data to determine tholeiitic or alkalic parentage of the xenoliths is complicated by the possibility that the clinopyroxene could represent either a cumulus mineral in equilibrium with the parental magma or a crystallized portion of the magma itself. In the latter case, the clinopyroxene could crystallize interstitially from trapped melt or as an adcumulus overgrowth on cumulus clinopyroxene. If the clinopyroxene is a cumulus mineral without postcumulus overgrowth, REE distribution coefficients could be used to calculate REE concentrations in the parental magmas, and these concentrations could then be compared with REE concentrations in Hualalai alkalic and tholeiitic lavas. However, if the clinopyroxene is partly or completely the result of

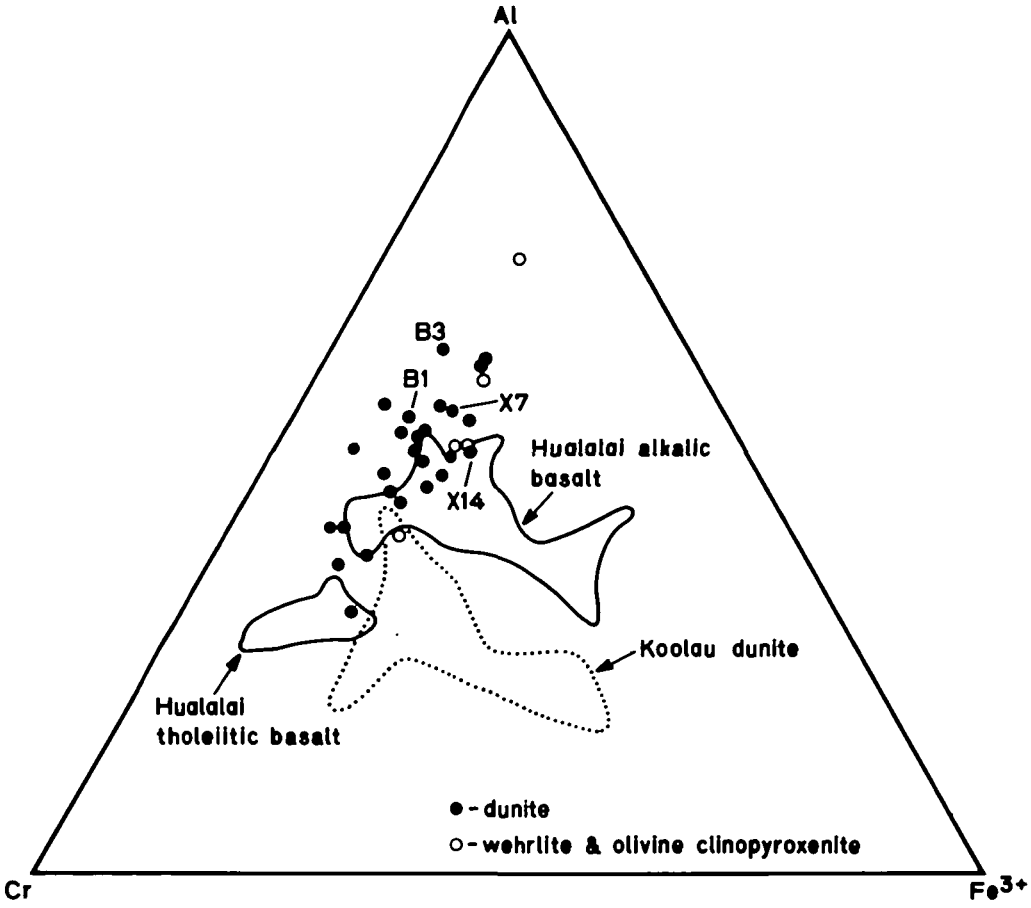

FIG. 8. Comparison of spinel compositions (cation ratios) in Kaupulehu ultramafic xenoliths (data from Tables 4 and 5) with those in Hualalai alkalic and tholeiitic basalts (data from Bohrson & Clague (1988) and Koolau dunite xenoliths (data from Sen & Presnall, 1986).

postcumulus crystallization, comparison of REE concentrations would be complicated by the possibility that part or all of the clinopyroxene would represent an unknown percentage of the magma, and its REE concentrations would be unrepresentative of the entire magma.

Mineralogical and phase equilibrium data provide some evidence on the cumulus or postcumulus origin of the clinopyroxene. On the basis of phase equilibrium relationships from 1 atm to 20 kb (Osborn & Tait, 1952; Presnall, 1966; Presnall *et al.*, 1978), clinopyroxene and olivine coprecipitate in proportions overwhelmingly dominated by clinopyroxene (80:20 to 90:10). Cumulates in layered intrusions such as the Duke Island complex, Alaska, and the Muskox intrusion in Canada confirm this relationship (Irvine, 1963, 1979). Thus, the very small amounts of clinopyroxene typically found in the Kaupulehu dunite xenoliths probably crystallized from liquid trapped between the cumulus olivine grains. In contrast, the large percentages of clinopyroxene in the wehrlite and clinopyroxenite xenoliths are consistent with a cumulus origin. In dunite samples AA, B4, and X14, the high percentage of clinopyroxene grains (5–8%), the blocky shapes of these grains, and the relatively forsterite-poor ($Fo_{81.4-84.2}$) olivine compositions suggest that these xenoliths represent a transition toward an olivine–clinopyroxene cumulus assemblage.

To evaluate the bearing of the REE data on the cumulus vs. postcumulus origin of the clinopyroxene, we examine the consequences of assuming, contrary to the phase equilibrium and textural evidence presented above, that the clinopyroxene in all the xenoliths is purely cumulus. On this assumption, distribution coefficients can be used to calculate REE patterns for magmas that crystallized the clinopyroxenes, and these patterns can be compared with those of alkalic and tholeiitic lavas from Hualalai. For these calculations, we use the preferred distribution coefficients (D) of Frey *et al.* (1978). As pointed out by Frey *et al.*, these coefficients are near the lower limit of published values, but are preferred because any contamination of analyzed mineral grains would lead to high values. Also, the Frey *et al.* preferred values are consistent with experimentally determined values of 0·19 for D_{Yb} (Watson *et al.*, 1987), 0·16 for D_{Gd} (Green *et al.*, 1971), and 0·13 for D_{Sm} (Ray *et al.*, 1983).

Figure 9 shows that the calculated REE patterns of presumed magmas that crystallized clinopyroxenes in the wehrlite and clinopyroxenite samples are approximately parallel to those of Hualalai alkalic lavas (Clague *et al.*, 1980*b*) but are at higher concentrations. Because REE concentrations of Hawaiian tholeiitic lavas typically are lower than those of Hawaiian alkalic lavas, the match of the calculated liquids with tholeiitic lavas would be even worse. One might argue that the presence of phenocrysts in the lavas analyzed by

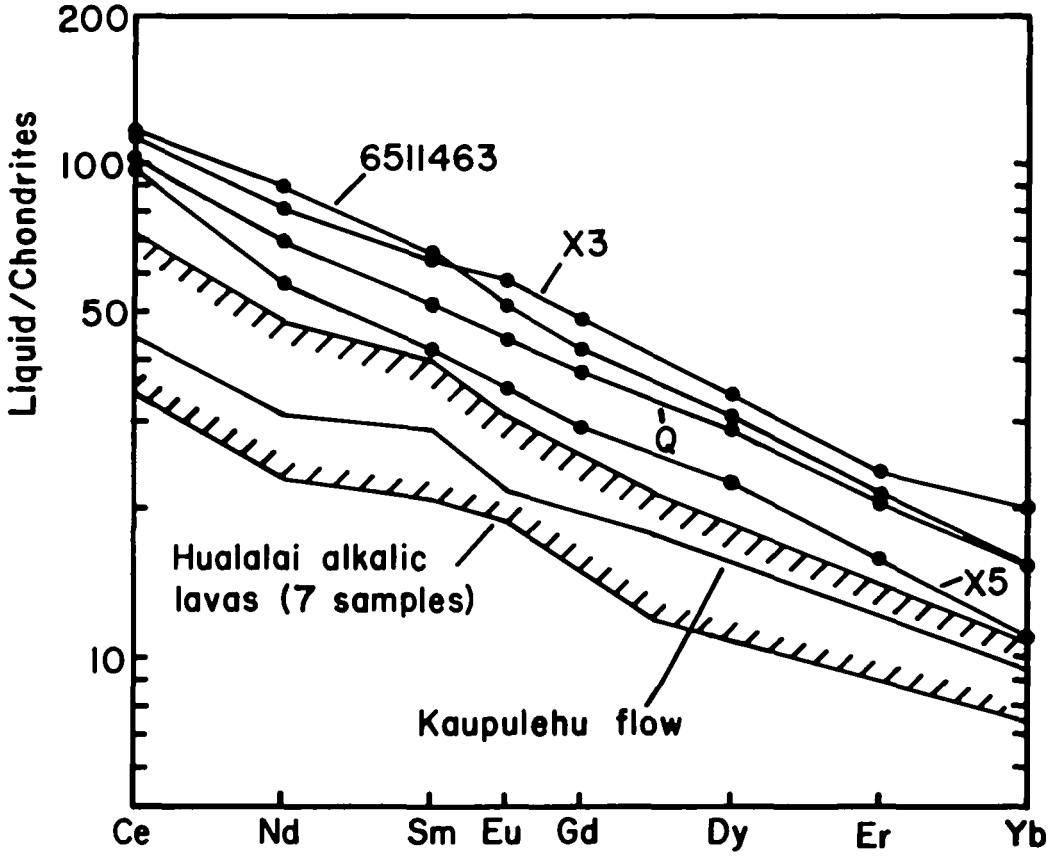

FIG. 9. Calculated REE patterns for liquids in equilibrium with Kaupulehu wehrlite and clinopyroxenite xenoliths based on the preferred distribution coefficients of Frey *et al.* (1978). Data for Hualalai mafic alkalic lavas are seven samples from Clague *et al.* (1980*a*) and two samples from Lofgren *et al.* (1981).

Clague *et al.* (1980*b*) could raise the REE concentrations in the liquid fraction sufficiently to overlap the concentrations of the calculated liquid compositions. In fact, the phenocryst proportions range from 5 to 15% (D. A. Clague, pers. comm.) and the REE patterns of the lavas reported by Clague *et al.* would be raised only an insignificant amount. The presumed magmas that crystallized clinopyroxenes in the dunite samples are even more enriched in REE. Thus, the REE data are inconsistent with a purely cumulus origin for any of the clinopyroxenes. At least some postcumulus overgrowth must have occurred, even for the samples with the lowest REE concentrations.

Figure 5 shows that REE patterns for clinopyroxene from the wehrlite and clinopyroxenite samples are strongly convex upward and lie at lower concentrations than those of typical Hawaiian tholeiites (Lofgren *et al.*, 1981) and Hualalai alkalic lavas (compare Figs. 5 and 8). Therefore, although the REE data require at least some postcumulus crystallization, they are consistent with the conclusion based on phase equilibrium and textural arguments that the clinopyroxene in these xenoliths is cumulus. Clinopyroxene separates from dunite samples B1, B3, and X7 have REE concentrations that fall generally in the range of those for Hualalai alkalic lavas (compare Figs. 5 and 8) and Hawaiian tholeiitic lavas (Lofgren *et al.*, 1981), and are higher than those from the wehrlite and clinopyroxenite xenoliths (Fig. 5). This relationship is consistent with crystallization of these clinopyroxenes as a postcumulus mineral interstitial to cumulus olivine.

The REE pattern for clinopyroxene from dunite sample X14 differs from those of clinopyroxenes from the other dunite samples and shows the LREE depletion and generally lower REE concentrations typical of clinopyroxene from the wehrlite and clinopyroxenite samples (Fig. 5). This feature is consistent with the earlier interpretation, based on petrography and mineralogy, that this sample represents the transition between postcumulus crystallization of clinopyroxene in the dunite xenoliths to cumulus crystallization in the wehrlite and clinopyroxenite xenoliths.

One dunite xenolith, sample B1, has clinopyroxene REE concentrations higher than those of typical Hawaiian tholeiites (Lofgren *et al.*, 1981), which indicates that the parental magma for this xenolith was alkalic. This is the only sample in which the REE data help to clarify the alkalic or tholeiitic character of the parental magma.

Isotopic data

Helium, strontium, and neodymium isotopic data exist both for xenoliths from the Kaupulehu flow and for Hualalai lavas. Kurz *et al.* (1983) found three dredged tholeiites from Hualalai to have $^3He/^4He$ values ranging from 14·4 to 17·6 times the atmospheric ratio. Ten alkalic lavas, also from Hualalai, were found to have much lower values, ranging from 7·84 to 9·84 × atmospheric (Kurz *et al.*, 1990). Data for five Kaupulehu xenoliths from Kurz *et al.* (1983), one from Rison & Craig (1983), and four from Kyser & Rison (1982) show a combined range of $^3He/^4He$ from 8·60 to 9·60 × atmospheric, all clearly within the alkalic range.

If the xenoliths were crystallized from tholeiitic Hualalai magmas, their present alkalic $^3He/^4He$ values might have been acquired by equilibration either with the lithosphere in which they crystallized ($^3He/^4He = 8 \times$ atmospheric) or with the host alkalic magma that transported them to the Earth's surface, or both. To evaluate these possibilities, we use the data of Hart (1984) for diffusion of He in olivine. Tholeiitic volcanism at Hualalai began $\sim 500\,000$ years ago (Clague & Dalrymple, 1987), so we assume a conservative age of $t = 500\,000$ years for formation of the xenoliths. If the temperature of the lithosphere is taken as 1100 °C (approximately just below the solidus temperature of basalt at 5–10 kb), the diffusion coefficient, D, of He in olivine is $\sim 2 \times 10^{-12}$ cm^2 s (Hart, 1984). Then

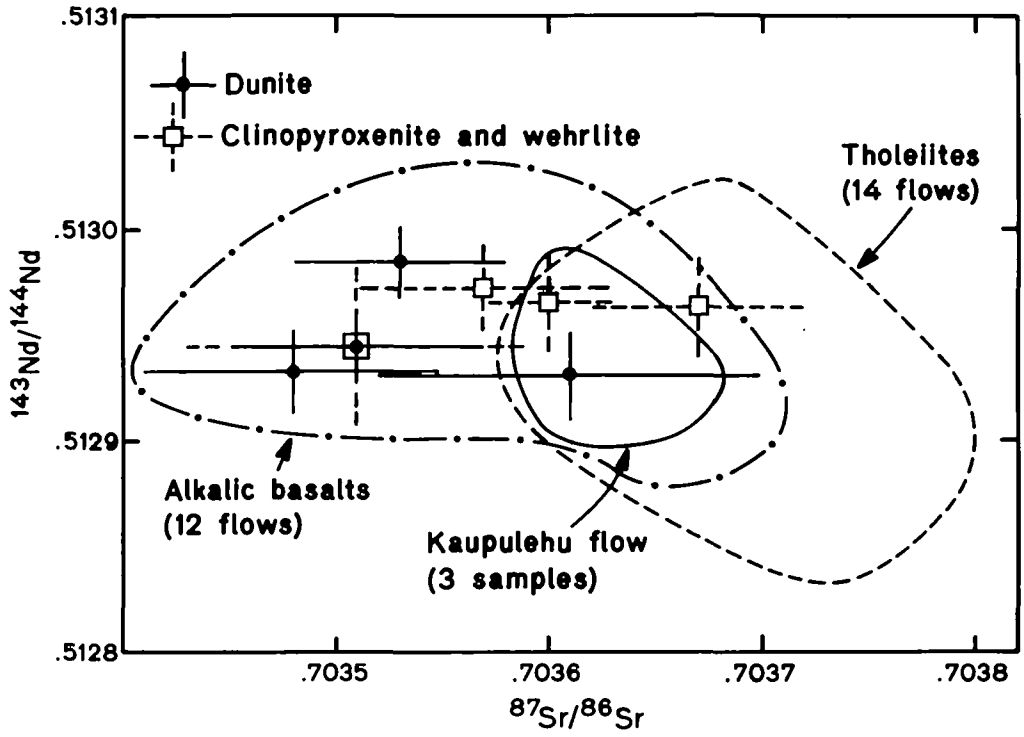

FIG. 10. Comparison of Nd and Sr isotopic compositions for clinopyroxenes from Kaupulehu xenoliths (Table 9) with those of tholeiitic and alkalic lavas from Hualalai Volcano and the host Kaupulehu flow. Horizontal and vertical lines show analytical uncertainties. Fields for the lavas are from Stille *et al.* (1986) and K. H. Park & A. Zindler (pers. comm.) and include the uncertainties in their analyses.

the characteristic transport distance for diffusion [$X = \sqrt{(Dt)}$] is ~0·2 mm (Hofmann & Hart, 1978). Thus, $^3He/^4He$ in dunite cumulates would not be significantly affected by exchange with the surrounding mantle.

Helium isotope exchange with the host magma can be evaluated in a similar way. For this calculation, we assume a magma temperature of 1200 °C ($D = 3 \times 10^{-10}$ cm^2 s) and a xenolith diameter of 1–35 cm, the size range of xenoliths from the 1800 Kaupulehu flow (Clague, 1987). The time required for equilibration of $^3He/^4He$ would then range from 25 years to 32 000 years, depending on the size of the xenolith. The maximum exposure time of the xenoliths to the host magma can be estimated from a calculation of the minimum magma flow velocity required to counteract the settling velocity of the largest xenoliths and bring them to the Earth's surface. By this procedure, Spera (1980) found a minimum magma velocity of 1·7 km/h for the 1800 Kaupulehu magma. If the xenoliths were entrained from a maximum depth of 30 km, the maximum magma exposure time during transport to the Earth's surface would be only ~18 h. Thus, essentially no helium isotope exchange would have occurred between the magma and the xenoliths. We conclude that the helium isotopic ratios of the xenoliths are representative of their magmatic origin and are a very strong constraint indicating that the parental magmas were alkalic.

Figure 10 shows that on an $^{87}Sr/^{86}Sr$ vs. $^{143}Nd/^{144}Nd$ plot, all the ultramafic xenoliths lie in the field of alkalic Hualalai lavas. Three of the dunites (B1, B3, and X7) have an unambiguous Hualalai alkalic signature; the rest could be derived from either alkalic or

tholeiitic Hualalai magmas. None of the xenoliths have an unambiguous tholeiitic signature. The three dunites with a clear alkalic identity are also isotopically distinct from their host Kaupulehu lava (Fig. 10) and therefore were not crystallized from it. This suggests that the other xenoliths with isotopic compositions analytically indistinguishable from that of the Kaupulehu lava also may not have crystallized from it. In particular, the one dunite xenolith (sample B1) having isotope ratios within the Kaupulehu field has a texture that shows deformation, which clearly indicates a history before being picked up by the Kaupulehu magma.

Multiple parental magmas

Bohrson & Clague (1988) observed two sequences of crystallization in the Kaupulehu ultramafic xenoliths showing pyroxene exsolution. One order is: spinel; olivine; orthopyroxene; clinopyroxene; plagioclase. The other is the same except that the two pyroxenes appear simultaneously. This difference suggests more than one parental magma. The ultramafic xenoliths without pyroxene exsolution studied here show a third sequence: spinel; olivine; clinopyroxene. Of particular significance is the fact that the xenoliths studied by Bohrson & Clague (1988) have a range of clinopyroxene *mg* values (82·4–85·5) that is completely overlapped by those in the wehrlite and clinopyroxenite samples we have studied (79·5–85·7). The former contain cumulus orthopyroxene; the latter do not. Therefore, more than one parental magma is required. Finally, multiple parental magmas are indicated by the isotopic heterogeneity of the clinopyroxenes. Figure 6 and Table 9 show that clinopyroxene in dunite X7, dunite B3, and clinopyroxenite X3 are distinct on an $^{87}Sr/^{86}Sr$ vs. $^{143}Nd/^{144}Nd$ plot.

Bohrson & Clague (1988) argued convincingly for a tholeiitic parental magma for the xenoliths with pyroxene exsolution on the basis that they contain cumulus enstatite. This conclusion is consistent with phase relationships both for natural tholeiite (Green & Ringwood, 1967) and for model system tholeiites (Presnall *et al.*, 1978, 1979; Sen & Presnall, 1984; Presnall & Hoover, 1987; Liu & Presnall, 1990) as long as the pressure does not exceed ~11 kb. However, Bohrson & Clague (1988, p. 139) noted that these xenoliths comprise only ~1% of the total xenolith population. Dunites, wehrlites, and olivine clinopyroxenites studied here make up ~60% of the xenolith population (Jackson *et al.*, 1981), and because they do not have cumulus orthopyroxene, we believe that their parentage must be considered separately.

Although we argue for the existence of multiple parental magmas, several features of the dunite, wehrlite, and olivine clinopyroxenite xenoliths support a coherent and common type of origin that involves sequential crystallization of dunite, wehrlite, and olivine clinopyroxenite cumulates from alkalic to transition parental magmas. These features, some of which have already been discussed, are summarized as follows.

(1) Olivine and clinopyroxene compositions are generally more magnesian in the dunites than in the wehrlites and olivine clinopyroxenites (Figs. 2 and 3), but a region of overlap occurs. This region is marked by iron-rich dunites with blocky clinopyroxenes that are possibly cumulus in origin. We have not found this textural feature among the more magnesian dunite samples.

(2) On a plot of modal percent clinopyroxene in dunite vs. percent forsterite in olivine, a large scatter occurs; but the maximum percent clinopyroxene increases as the percent forsterite decreases (Tables 1 and 2). This is consistent with the introduction of small amounts of cumulus clinopyroxene in the more iron-rich dunites.

(3) Dunite sample X14, which has very iron-rich olivine ($Fo_{81\cdot4}$) and clinopyroxene that appears to be cumulus, has a clinopyroxene REE plot like those for clinopyroxenes from the

wehrlite and olivine clinopyroxenite samples. Thus, it appears to represent the transition between more magnesian dunite cumulates and the wehrlite–clinopyroxenite suite of cumulates.

(4) Spinel compositions are similar in all the xenoliths but are generally more magnesian in the dunites than in the wehrlites and olivine clinopyroxenites (Fig. 7). This difference is consistent with differences in the olivine and clinopyroxene compositions.

(5) Spinel compositions indicate that the parental magmas were alkalic to transitional. Clinopyroxene compositions are not as definitive but are also consistent with this interpretation.

(6) He and Sr isotope ratios both indicate alkalic to transitional parental magmas for the xenoliths, and the slight heterogeneity of Sr isotope ratios indicates several parental magmas.

CONCLUDING STATEMENT

The samples from the xenolith beds of the 1800 Kaupulehu flow that we have studied are far from an exhaustive representation of this rich and diverse accumulation of xenoliths. It is clear, both from our work and previous studies, that the magma sampled a wide range of materials including cumulates from both alkalic (this study) and tholeiitic (Bohrson & Clague, 1988) magma chambers and even an occasional fragment of oceanic crust (Clague & Chen, 1986). The locality represents a superb, but scrambled, sample of the deep interior of a mature Hawaiian volcano down to a depth of perhaps 30 km, and it deserves much more thorough documentation.

Our conclusion regarding alkalic parental magmas stands in contrast to the conclusion of Sen & Presnall (1986) that the dunite xenoliths from Koolau volcano on Oahu have a tholeiitic parentage. An interesting difference between the two dunite suites is the generally higher Al_2O_3 content of clinopyroxenes in the dunites from Hualalai (2·48–7·02%) relative to those from Koolau (1·37–2·67%), which suggests a different origin for the two suites. The difference could be caused by higher pressures of formation for the Kaupulehu xenoliths (O'Hara, 1967) or crystallization from more aluminous parental magmas. We have also noted that spinels from the Hualalai dunites have lower Cr/(Cr + Al) than those from the Koolau dunites.

Extensive crystallization of olivine in the absence of pyroxenes and plagioclase has long been recognized to be an important part of the crystallization history of Hawaiian tholeiites (Macdonald, 1949; Powers, 1955; Wright, 1971) but it has not previously been recognized to be important for Hawaiian alkalic magmas. Data presented here plus data from two other Hawaiian volcanoes, Loihi (Clague, 1988) and Mauna Kea (Atwill & Garcia, 1985), strongly indicate that it should be so recognized. Experimental data (Presnall *et al.*, 1978, 1979; Presnall & Hoover, 1987) indicate that increasing alkalinity of the magma would progressively reduce its capacity for crystallization of olivine alone before the crystallization of clinopyroxene, but that this capacity still exists even for nepheline-normative magmas. Our results combined with data for xenoliths from other Hawaiian volcanoes (for example, Sen & Presnall, 1986; Clague, 1988; Sen, 1988) indicate that significant portions of the deep cores of Hawaiian volcanoes consist of ultramafic cumulates crystallized both from tholeiitic and from alkalic magmas.

ACKNOWLEDGEMENTS

This work was supported by National Science Foundation Grants EAR-8018359, EAR-8212889, and EAR 8418685 to Presnall, and OCE-8415759 to Stern. We thank A. Zindler

for providing access to his laboratory and for assistance with the Nd isotope analyses; K.-H. Park, G. Worner, A. Zindler, and D. Clague for permission to use unpublished Sr and Nd isotope data on Hualalai lavas; and D. A. Clague and W. G. Melson for facilitating access to the Jackson xenolith collection at the Smithsonian Institution, Washington, DC. We thank D. A. Clague for numerous conversations and two very helpful reviews at different stages of manuscript preparation, and we thank T. N. Irvine for helpful comments regarding cumulus textures. Journal reviews by A. Basu, M. O. Garcia, T. N. Irvine, and especially F. A. Frey led to significant improvements in the final manuscript. This paper is Contribution 526 of the Geosciences Program, The University of Texas at Dallas.

REFERENCES

Albee, A. L., & Ray, L., 1970. Correction factors for electron-probe microanalysis of silicates, oxides, carbonates, phosphates and sulfates. *Anal. Chem.* **42**, 1408–14.

Arai, S., & Fujii, T., 1979. Petrology of ultramafic rocks from site 395. *Initial Reports of the Deep Sea Drilling Project, 45.* Washington, DC: U.S. Government Printing Office, 587–94.

Arth, J. G., 1976. Behavior of trace elements during magmatic process—a summary of theoretical models and their application. *J. Res. U.S. Geol. Surv.* **4**, 41–7.

Atwill, T. M., & Garcia, M. O., 1985. Petrogenesis of ultramafic xenoliths from Mauna Kea: mantle or crust origin. *Trans. Am. Geophys. Union* **66**, 1133.

Basu, A. R., & Murthy, V. R., 1977. Ancient lithospheric lherzolite xenoliths in alkali basalt from Baja California. *Earth Planet. Sci. Lett.* **35**, 239–46.

Beeson, A. E., 1976. Petrology, mineralogy, and geochemistry of the East Molokai volcanic series, Hawaii. *U.S. Geol Surv. Prof. Paper* **961**.

Bence, A. E., & Albee, A. L., 1968. Empirical correction factors in electron microanalysis of silicates and oxides. *J. Geol.* **76**, 382–403.

Bohrson, W. A., & Clague, D. A., 1988. Origin of ultramafic xenoliths containing exsolved pyroxenes from Hualalai Volcano, Hawaii. *Contr. Miner. Petrol.* **100**, 139–55.

Bonatti, E., Ottonello, G., & Hamlyn, P. R., 1986. Peridotites from the island of Zabargad (St. John), Red Sea: petrology and geochemistry. *J. Geophys. Res.* **91**, 599–631.

Carter, J. L., 1970. Mineralogy and chemistry of the earth's upper mantle based on the partial fusion–partial crystallization model. *Bull. Geol. Soc. Am.* **88**, 556–70.

Chen, C.-Y., & Frey, F. A., 1985. Trace element and isotopic geochemistry of lavas from Haleakala Volcano, East Maui, Hawaii. *J. Geophys. Res.* **90**, 8743–68.

Clague, D. A., 1987. Hawaiian xenolith populations, magma supply rates, and development of magma chambers. *Bull. Volcanol.* **49**, 577–87.

—— 1988. Petrology of ultramafic xenoliths from Loihi Seamount, Hawaii. *J. Petrology* **29**, 1161–86.

—— Chen, C.-H., 1986. Ocean crust xenoliths from Hualalai Volcano, Hawaii. *Geol. Soc. Am. Abstr. Prog.* **18**, 565.

—— Dalrymple, G. B., 1987. The Hawaiian–Emperor volcanic chain. Part I. Geologic evolution. In: Decker, R. W., Wright, T. L., & Stauffer, P. H. (eds.) *Volcanism in Hawaii. U.S. Geol Surv. Prof. Paper* **1350**, 5–54.

—— Fisk, M. R., & Bence, A. E., 1980*a*. Mineral chemistry of basalts from Ojin, Nintoku, and Suiko seamounts, leg 55, DSDP. *Initial Reports of the Deep Sea Drilling Project, 55.* Washington, DC: U.S. Government Printing Office, 607–37.

—— Jackson, E. D., & Wright, T. L., 1980*b*. Petrology of Hualalai Volcano: implication for mantle composition. *Bull. Volcanol.* **43**, 641–56.

Clarke, D. B., & Loubat, H., 1977. Mineral analyses from the peridotite–gabbro–basalt complex at site 334, DSDP leg 37. *Initial Reports of the Deep Sea Drilling Project, 37.* Washington, DC: U.S. Government Printing Office, 847–55.

Dick, H. J. B., 1989. Abyssal peridotites, very slow spreading ridges and ocean ridge magmatism. In: Saunders, A. D., & Norry, M. J. (eds.) *Magmatism in the Ocean Basins. Geol. Soc. Spec. Publ.* **42**, 71–105.

—— Bullen, T., 1984. Chromium spinel as a petrogenetic indicator in oceanic environments. *Contr. Miner. Petrol.* **86**, 54–76.

—— Fisher, R. L., 1984. Mineralogical studies of the residues of mantle melting: abyssal and alpine peridotites. In: Kornprobst, J. (ed.) *Kimberlites II: The Mantle and Crust–Mantle Relationships.* Amsterdam: Elsevier, 295–308.

Ehrenberg, S. N., 1982. Rare earth element geochemistry of garnet lherzolite and megacrystalline nodules from minette of the Colorado Plateau. *Earth Planet. Sci. Lett.* **57**, 191–210.

Engi, M., 1983. Equilibria involving Al–Cr spinel: Mg–Fe exchange with olivine: experiments, thermometric analysis, and consequences for geothermometry. *Am. J. Sci.* **283-A**, 29–71.

Evans, B. W., & Wright, T. L., 1972. Composition of liquidus chromite from the 1959 (Kilauea Iki) and 1965 (Makaopuhi) eruptions of Kilauea volcano, Hawaii. *Am. Miner.* **57**, 217–30.

Fabries, J., 1979. Spinel–olivine geothermometry in peridotites from ultramafic complexes. *Contr. Miner. Petrol.* **69**, 329–36.

Feigenson, M. D., Hofmann, A. W., & Spera, F. J., 1983. Case studies on the origin of basalt. II. The transition from tholeiite to alkalic volcanism on Kohala Volcano, Hawaii. *Ibid.* **84**, 390–405.

Flanagan, E. J., 1973. 1972 values for international geochemical reference standards. *Geochim. Cosmochim. Acta* **37**, 1189–200.

Fodor, R. V., Keil, K., & Bunch, T. E., 1975. Contributions to the mineral chemistry of Hawaiian rocks IV. Pyroxenes in rocks from Haleakala and West Maui Volcanos, Maui, Hawaii. *Contr. Miner. Petrol.* **50**, 173–95.

Frey, F. A., Green, D. H., & Roy, S. D., 1978. Integrated models of basalt petrogenesis: a study of quartz tholeiites to olivine melilitites from South Eastern Australia utilizing geochemical and experimental petrological data. *J. Petrology* **19**, 453–513.

Fujii, T., 1978. Fe–Mg partitioning between olivine and spinel. *Carnegie Inst. Wash. Yearb.* **76**, 563–9.

Gladney, E. S., Burns, C. E., & Roelandts, I., 1983. 1982 compilation of elemental concentrations in eleven United States Geological Survey rock standards. *Geostand. Newslett.* **7**, 3–226.

Green, D. H., & Hibberson, W. O., 1976. The instability of plagioclase in peridotite at high pressure. *Lithos* **3**, 209–21.

—— Ringwood, A. E., 1967. The genesis of basaltic magmas. *Contr. Miner. Petrol.* **15**, 103–90.

———— Ware, N. G., Hibberson, W. O., Major, A., & Kiss, E., 1971. Experimental petrology and petrogenesis of Apollo 12 basalts. *Proc. Second Lunar Sci. Conf.* **1**, 601–15.

Green, H. W., 1979. Trace elements in the fluid phases of the Earth's mantle. *Nature* **227**, 465–7.

Hamlyn, P. R., & Bonatti, E., 1980. Petrology of mantle-derived ultramafics from the Owen Fracture Zone, Northwest Indian Ocean: implications for the nature of the oceanic upper mantle. *Earth Planet. Sci. Lett.* **48**, 65–79.

Hart, S. R., 1971. K, Rb, Cs, Sr and Ba contents and Sr isotope ratios of ocean floor basalt. *Phil. Trans. R. Soc. Lond.* **A268**, 573–87.

—— 1984. He diffusion in olivine. *Earth Planet. Sci. Lett.* **70**, 297–302.

Hebert, R., Bideau, D., & Hekinian, R., 1983. Ultramafic and mafic rocks from the Garret Transform Fault near 13°30'S on the East Pacific Rise: igneous petrology. *Ibid.* **65**, 107–25.

Hofmann, A. W., & Hart, S. R., 1978. An assessment of local and regional isotopic equilibrium in the mantle. *Ibid.* **38**, 44–62.

Irvine, T. N., 1963. Origin of the ultramafic complex at Duke Island, southeastern Alaska. *Miner. Soc. Am. Spec. Paper* **1**, 36–45.

—— 1979. Rocks whose composition is determined by crystal accumulation and sorting. In: *The Evolution of the Igneous Rocks: Fiftieth Anniversary Perspectives.* Princeton: Princeton University Press, 245–306.

Irving, A., & Frey, F. A., 1984. Trace element abundances in megacrysts and their host basalts: constraints on partition coefficients and megacryst genesis. *Geochim. Cosmochim. Acta* **48**, 1201–21.

Jackson, E. D., 1968. The character of the lower crust and upper mantle beneath the Hawaiian Islands. *Proc. XXIII Int. Geol. Congr.* **1**, 135–50.

—— 1969. Chemical variation in coexisting chromite and olivine in chromitite zones of the Stillwater complex. *Econ. Geol. Mon.* **4**, 41–71.

—— Clague, D. A., 1981. The nodule beds of 1800–1801 Kaupulehu flow, Hualalai Volcano, Hawaii. *U.S. Geol. Surv. Misc. Field Studies Map MF-1355.*

—— Clague, D. A., Engleman, E., Friesen, W. B., & Norton, D., 1981. Xenoliths in the alkalic basalt flows from Hualalai Volcano, Hawaii. *U.S. Geol. Surv. Open-File Rep.* **81-1031.**

Kaneoka, I., & Takaoka, N., 1978. Excess ^{129}Xe and high $^{3}He/^{4}He$ ratios in olivine phenocrysts of Kapuho lava and xenolithic dunites from Hawaii. *Earth Planet. Sci. Lett.* **39**, 382–6.

———— 1980. Rare gas isotopes in Hawaiian ultramafic nodules and volcanic rocks: constraint on genetic relationship. *Science* **208**, 1366–8.

Kirby, S. H., & Green, H. W., III, 1980. Dunite xenoliths from Hualalai Volcano: evidence for mantle diapiric flow beneath the island of Hawaii. *Am. J. Sci.* **280-A**, 550–75.

Kretz, R., 1982. Transfer and exchange equilibria in a portion of the pyroxene quadrilateral as deduced from natural and experimental data. *Geochim. Cosmochim. Acta* **46**, 411–21.

Kurz, M. D., Colodner, D., Trull, T. W., Moore, R. B., & O'Brien, K., 1990. Cosmic ray exposure dating with *in situ* produced cosmogenic ^{3}He: results from young Hawaiian lava flows. *Earth Planet. Sci. Lett.* **97**, 177–89.

—— Garcia, M. O., Frey, F. A., & O'Brien, P. A., 1987. Temporal helium isotopic variations within Hawaiian volcanoes: basalts from Mauna Loa and Haleakala. *Ibid.* **51**, 2905–14.

—— Jenkins, W. J., Hart, S. R., & Clague, D. A., 1983. Helium isotopic variations in volcanic rocks from Loihi Seamount and the Island of Hawaii. *Ibid.* **66**, 388–406.

Kyser, T. K., & Rison, W., 1982. Systematic of rare gas isotopes in basic lavas and ultramafic xenoliths. *J. Geophys. Res.*. **87**, 5611–30.

Lindsley, D. H., & Andersen, D. J., 1983. A two-pyroxene thermometer. *Ibid.* **88**, A887–906.

Liu, T.-C., & Presnall, D. C., 1990. Liquidus phase relationships on the join anorthite–forsterite–quartz at 20 kbar with applications to basalt petrogenesis and igneous sapphirine. *Contr. Miner. Petrol.* **104**, 735–42.

Lofgren, G. G., Bence, A. E., Duke, M. B., Dungan, M. A., Green, J. C., Haggerty, S. E., Haskin, L. A., Irving, A. J.,

Lipman, P. W., Naldrett, A. J., Papike, J. J., Reid, A. M., Rhodes, J. M., Taylor, S. R., & Vaniman, D. T., 1981. Petrology and chemistry of terrestrial, lunar and meteoritic basalts. In: *Basaltic Volcanism on the Terrestrial Planets.* New York: Pergamon Press, 132–60.

Lupton, J. E., & Garcia, M. O., 1986. Helium isotopes in submarine basalts from the island of Hawaii. *Trans. Am. Geophys. Union* **67**, 1271.

Macdonald, G. A., 1949. Hawaiian petrographic province. *Bull. Geol. Soc. Am.* **60**, 1541–96.

Mathez, E. A., Dietrich, V. J., & Irving, A. J., 1984. The geochemistry of carbon in mantle peridotites. *Geochim. Cosmochim. Acta* **48**, 1849–60.

Mercier, J.-C. C., & Nicolas, A., 1975. Textures and fabrics of upper-mantle peridotites as illustrated by xenoliths from basalts. *J. Petrology* **16**, 454–87.

Moore, R. B., Clague, D. A., Rubin, M., & Bohrson, W. A., 1987. Hualalai Volcano: a preliminary summary of geologic, petrologic, and geophysical data. *U.S. Geol. Surv. Prof. Paper* **1350**, 571–86.

Mysen, B. O., 1976. Experimental determination of some geochemical parameters relating to conditions of equilibration of peridotite in the upper mantle. *Am. Miner.* **61**, 677–83.

—— 1979. Trace-element partitioning between garnet peridotite minerals and water-rich vapor: experimental data from 5 to 30 kb. *Am. Miner.* **64**, 274–87.

O'Donnell, T. H., & Presnall, D. C., 1980. Chemical variations of the glass and mineral phases in basalts dredged from 25°–30 °N along the Mid-Atlantic Ridge. *Am. J. Sci.* **280-A**, 845–68.

O'Hara, M. J., 1967. Mineral parageneses in ultrabasic rocks. In: Wyllie, P. J. (ed.) *Ultramafic and Related Rocks.* New York: John Wiley, 393–403.

Osborn, E. F., & Tait, D. B., 1952. The system diopside–forsterite–anorthite. *Am. J. Sci.* Bowen Vol., 413–33.

Pike, J. E. N., & Schwarzmann, E. C., 1977. Classification of textures in ultramafic xenoliths. *J. Geol.* **85**, 49–61.

Powers, H. A., 1955. Composition and origin of basaltic magma of the Hawaiian Islands. *Geochim. Cosmochim. Acta* **7**, 77–107.

Presnall, D. C., 1966. The join forsterite–diopside–iron oxide and its bearing on the crystallization of basaltic and ultramafic magmas. *Am. J. Sci.* **264**, 753–809.

—— Dixon, J. R., O'Donnell, T. H., & Dixon, S. A., 1979. Generation of mid-ocean ridge tholeiites. *J. Petrology* **20**, 3–35.

—— Dixon, S. A., Dixon, J. R., O'Donnell, T. H., Brenner, N. L., Schrock, R. L., & Dycus, D. W., 1978. Liquidus phase relations on the join diopside–forsterite–anorthite from 1 atm to 20 kbar: their bearing on the generation and crystallization of basaltic magma. *Contr. Miner. Petrol.* **66**, 203–20.

—— Hoover, J. D., 1987. High pressure phase equilibrium constraints on the origin of mid-ocean ridge basalts. In: Mysen, B. O. (ed.) *Magmatic Processes: Physicochemical Principles. Geochem. Soc. Spec. Publ.* **1**, 75–88.

Prinz, M., Keil, K., Green, J. A., Reid, A. M., Bonatti, E., & Honnorez, J., 1976. Ultramafic and mafic dredged samples from the Equatorial Mid-Atlantic Ridge and fracture zones. *J. Geophys. Res.* **81**, 4087–103.

Ray, G. L., Shimizu, N., & Hart, S. R., 1983. An ion microprobe study of the partitioning of trace elements between clinopyroxene and liquid in the system diopside–albite–anorthite. *Geochim. Cosmochim. Acta* **47**, 2131–40.

Richter, D. H., & Murata, K. J., 1961. Xenoliths nodules in the 1800–1801 Kaupulehu flow of Hualalai Volcano. *U.S. Geol. Surv. Prof. Paper* **424B**, B215–17.

Ringwood, A. E., 1975. *Composition and Petrology of the Earth's Mantle.* New York: McGraw–Hill.

Rison, W., & Craig, H., 1983. Helium isotopes and mantle volatiles in Loihi Seamount and Hawaiian Island basalts and xenoliths. *Earth Planet. Sci. Lett.* **66**, 407–26.

Roden, M. F., Frey, F. A., & Clague, D. A., 1984. Geochemistry of tholeiitic and alkalic lavas from the Koolau Range, Oahu, Hawaii: implications for Hawaiian volcanism. *Ibid.* **69**, 141–58.

Roedder, E., 1965. Liquid CO_2 inclusions in olivine-bearing nodules and phenocrysts from basalts. *Am. Miner.* **50**, 1746–82.

Roeder, P. L., Campbell, I. M., & Jamieson, H. E., 1979. A re-evaluation of the olivine–spinel thermometry. *Contr. Miner. Petrol.* **68**, 325–34.

Schneider, M. E., & Eggler, D. H., 1986. Fluids in equilibrium with peridotite minerals: implications for mantle metasomatism. *Geochim. Cosmochim. Acta* **50**, 711–24.

Sen, G. 1988. Petrogenesis of spinel lherzolite and pyroxenite suite xenoliths from the Koolau shield, Oahu, Hawaii: implications for petrology of the post-eruptive lithosphere beneath Oahu. *Contr. Miner. Petrol.* **100**, 61–91.

—— Presnall, D. C., 1980. Dunite nodules from the Koolau shield, Hawaii: crystal cumulates from a tholeiitic magma chamber. *Geol. Soc. Am. Abstr. Prog.* **12**, 519.

———— 1984. Liquidus phase relationships on the join anorthite–forsterite–quartz at 10 kbar with applications to basalt petrogenesis. *Contr. Miner. Petrol.* **85**, 404–8.

———— 1986. Petrogenesis of dunite xenoliths from Koolau Volcano, Oahu, Hawaii: implications for Hawaiian volcanism. *J. Petrology* **27**, 197–217.

Shimizu, N., 1974. An experimental study of the partitioning of K, Rb, Cs, Sr and Ba between clinopyroxene and liquid at high pressure. *Geochim. Cosmochim. Acta* **38**, 1789–98.

Sigurdsson, H., 1977. Spinels in leg 37 basalts and peridotites: phase chemistry and zoning. *Initial Reports of the Deep Sea Drilling Project, 37.* Washington, DC: U.S. Government Printing Office, 883–91.

—— Schilling J.-G., 1976. Spinels in Mid-Atlantic ridge basalts: chemistry and occurrence. *Earth Planet. Sci. Lett.* **29**, 7–20.

Sinton, J. M., 1979. Petrology of (Alpine-type) peridotites from site 395, DSDP leg 45. *Initial Reports of the Deep Sea Drilling Project, 45*. Washington, DC: U.S. Government Printing Office, 595–601.

Spera, F. J., 1980. Aspects of magma transport. In: Hargraves, R. B. (ed.) *Physics of Magmatic Processes*. Princeton: Princeton University Press, 265–323.

Staudigel, H., Zindler, A., Hart, S. R., Leslie, T., Chen, C.-Y., & Clague, D. A., 1984. Systematics of a juvenile intraplate volcano: Pb, Nd, and Sr isotope ratios of basalts from Loihi Seamount, Hawaii. *Earth Planet. Sci. Lett.* **69**, 13–29.

Stern, R. J., & Bibee, L. D., 1984. Esmeralda Bank: geochemistry of an active submarine volcano in the Mariana Island Arc. *Contr. Miner. Petrol.* **86**, 159–69.

Stille, P., Unruh, D. M., & Tatsumoto, M., 1986. Pb, Sr, Nd, and Hf isotopic constraints on the origin of Hawaiian basalts and evidence for a unique mantle source. *Geochim. Cosmochim. Acta* **50**, 2303–19.

Sun, S. S., Nesbitt, R. W., & Sharaskin, A. Y., 1979. Geochemical characteristics of mid-ocean ridge basalts. *Earth Planet. Sci. Lett.* **44**, 119–38.

Symes, R. F., Beva, J. C., & Hutchison, R., 1977. Phase chemistry studies on gabbro and peridotite rocks from site 334, DSDP leg 37. *Initial Reports of the Deep Sea Drilling Project, 37*. Washington, DC: U.S. Government Printing Office, 841–5.

Takahashi, E., & Kushiro, I., 1983. Melting of a dry peridotite at high pressures and basalt magma genesis. *Am. Miner.* **68**, 859–79.

Watson, E. B., Othman, D. B., Luck, J. M., & Hofmann, A. W., 1987. Partitioning of U, Pb, Cs, Yb, Hf, Re and Os between chromian diopsidic pyroxene and haplobasaltic liquid. *Chem. Geol.* **62**, 191–208.

Wendlandt, R. F., & Harrison, W. J., 1979. Rare earth partitioning between immiscible carbonate and silicate liquids and CO_2 vapor: results and implication for the formation of light rare-earth enriched rocks. *Contr. Miner. Petrol.* **69**, 409–19.

White, R. W., 1966. Ultramafic inclusions in basaltic rocks from Hawaii. *Ibid.* **12**, 245–314.

Wright, T. L., 1971. Chemistry of Kilauea and Mauna Loa lava in space and time. *U.S. Geol. Surv. Prof. Paper* **735**, 40 pp.

Zindler, A., & Jagouts, E., 1988. Mantle cryptology. *Geochim. Cosmochim. Acta* **52**, 319–32.

——Staudigel, H., & Batiza, R., 1984. Isotope and trace element geochemistry of young Pacific seamounts: implications for the scale of upper mantle heterogeneity. *Earth Planet. Sci. Lett.* **70**, 175–95.

————Hart, S. R., Endres, R., & Goldstein, S., 1983. Nd and Sr isotopic study of a mafic layer from Ronda ultramafic complex. *Nature* **304**, 226–30.

APPENDIX A: ANALYTICAL METHODS

All mineral compositions were determined at the University of Texas at Dallas with an ARL-EMX electron microprobe equipped with a Tracor-Northern TN-2000 automation system. The accelerating potential was 15 kV, the beam current was 0·15–0·20 μA, and the beam diameter was < 1 μm. The data reduction procedure of Bence & Albee (1968) and the correction factors of Albee & Ray (1970) were used for all analyses. Each analysis listed in the tables is an average of 7–15 spot analyses.

For the isotopic and trace element analyses, the clinopyroxene separates from dunite, wehrlite, and olivine clinopyroxenite xenoliths were hand-picked, crushed in an agate mortar, and sieved. The 100–300 μm size fraction was then re-picked under 40 × magnification until no further impurities could be seen. To avoid possible altered materials and contamination along grain boundaries and mineral surfaces, acid washing was carried out by the procedure of Zindler & Jagouts (1988), as follows. The separates were sequentially washed ultrasonically in distilled water for 1 h, washed in hot (100 °C) 2·5 N HCl for 30 min, washed in cold (room temperature) 5% HF for 10 min, rinsed five times with cold 2·5 N HCl, and finally rinsed five times with distilled water. This procedure was established after the results of a leaching experiment outlined in Appendix B. Distilled reagents were used for the washing and other chemical procedures.

The trace element and Sr isotopic analyses were performed at the University of Texas at Dallas. Both 6-in (for K, Rb, and Sr contents and $^{87}Sr/^{86}Sr$) and 12-in (for REE and Ba contents) radius solid-source mass spectrometers were used. Eight clinopyroxene separates and the USGS standard BCR-1 were analyzed for REE, K, Rb, Sr, and Ba by isotope dilution after the methods of Hart (1971) and Shimizu (1974). For each clinopyroxene analysis, 400–600 mg of acid-washed sample were used. Values of $^{87}Sr/^{86}Sr$ were normalized to $^{86}Sr/^{88}Sr = 0{\cdot}11940$ and corrected relative to 0·70800 for the E + A $SrCO_3$ standard.

Neodymium isotopic measurements were carried out at Lamont–Doherty Geological Observatory of Columbia University, on a modified V.G. Micromass 30 mass spectrometer (Zindler *et al.*, 1984). Values of $^{143}Nd/^{144}Nd$ were normalized to $^{146}Nd/^{144}Nd = 0{\cdot}72190$ and corrected relative to 0·512645 for the BCR-1 standard.

TABLE A1

Trace element analyses of USGS standard BCR-1 basalt (ppm)

	(1)	(2)	(3)	(4)
K	13971	14130	14000	14000±700
Rb	47·6	47·4	46·6	47·1±0·6
Sr	327	329	330	330±5
Ba	670	682	675	678±16
Ce	53·5	53·9	53·9	53·7±0·8
Nd	28·3	28·54	29	28·7±0·6
Sm	6·59	6·45	6·6	6·58±0·17
Eu	1·91	2·00	1·94	1·96±0·05
Gd	6·56	6·67	6·6	6·68±0·13
Dy	6·29	6·06	6·3	6·35±0·12
Er	3·58	3·51	3·59	3·61±0·09
Yb	3·32	3·51	3·36	3·39±0·08

(1) This study, mean of three analyses except for Sr, Gd, and Yb (two analyses).
(2) Stern & Bibee (1984).
(3) Flanagan (1973).
(4) Consensus values (Gladney *et al.*, 1983).

The rare earth element and other trace element contents of the BCR-1 standard (Table A1) are in good agreement with those from other authors (Flanagan, 1973; Stern & Bibee, 1984) and the consensus values (Gladney *et al.*, 1983). Total blanks (in nanograms) determined at the University of Texas at Dallas are as follows: K (63), Rb (0·1), Sr (2·6), Ba (4·5), Ce (0·5), Nd (0·3), Sm (0·05), Gd (0·06), Er (0·05), and Yb (0·07).

APPENDIX B: SOURCES OF CONTAMINATION OF CLINOPYROXENE SEPARATES

Despite care taken to obtain the purest possible clinopyroxene separates, certain contaminants might contribute to their trace element contents. Potential contaminants are grain surface materials, glass or fluid inclusions, and other mineral inclusions such as amphibole, mica, or apatite. Possible grain surface materials could include basaltic glass that penetrated into the clinopyroxene during or after entrainment of the xenolith in the host magma or liquid trapped between mineral grains when crystallization or recrystallization occurred. Also, CO_2 and silicate glass inclusions (Roedder, 1965; Kirby & Green, 1980; Mathez *et al.*, 1984) may contain significant amounts of minor and trace elements such as K, Rb, La, Ce, and U (Green, 1979). Although Mysen (1979) and Wendlandt & Harrison (1979) suggested that CO_2-rich fluids are an important carrier of trace elements in the mantle, Schneider & Eggler (1986) argued that trace elements are not concentrated in H_2O–CO_2 fluids and instead are carried by silicate melts.

Basaltic glass and surface materials along grain boundaries can be dissolved easily in 2·5 N HCl and dilute 5% HF (Shimizu, 1974; Zindler *et al.*, 1983). In fact, analysis of leachates shows that even weak acids can remove K, Rb, Ba, La, Ce, and other elements that enter minerals in ultramafic rocks, and also can change Sr and Pb isotopic compositions (Basu & Murthy, 1977; Ehrenberg, 1982; Zindler *et al.*, 1983). To test for contamination by CO_2 and silicate glass inclusions, an acid leaching experiment was applied to the clinopyroxene separate from wehrlite sample X3. The separate was analyzed after initial washing in distilled water, then after washing in HCl and HF, and finally after crushing and washing again in HCl (Table B1). After the first acid washing, the separated clinopyroxene grains would be expected to be devoid of surface contamination, but CO_2 and silicate glass inclusions inside the clinopyroxene grains would still be intact. The final step of crushing and acid washing was designed to evaluate REE and other trace element contents in the inclusions.

The three analyses have almost identical REE contents (Table B1). A similar result on the La content in Hualalai ultramafic xenoliths was reported by Mathez *et al.* (1984). Except for Ce, the leachate has an REE pattern that is parallel to and below that of the clinopyroxene. The similarity of

TABLE B1

Trace element concentrations of wehrlite X3 clinopyroxene separate

	*After H_2O wash**	*After first acid wash†*	*After second acid wash‡*	*First leachate§*	*Calculated ‖ measured*
Ce	3·77	3·93	3·81	4·71	1·046
Nd	4·36	4·39	4·42	3·62	1·004
Sm	1·63	1·63	1·63	1·18	0·995
Eu	0·63	0·64	0·64	0·45	1·011
Gd	2·16	2·17	2·23	1·50	0·999
Dy	2·12	2·19	2·24	1·36	1·026
Er	1·04	1·04	1·08	0·64	0·993
Yb	0·78	0·81	0·84	0·45	1·031
K	42·6	24·1	21·8	1072	0·990
Rb	0·12	0·08	0·08	3·91	1·130
Sr	44·76	45·13	40·31	105·23	1·030
Ba	1·92	1·63	0·95	46·15	1·240

* Washed ultrasonically in distilled water for 1 h.

† Washed for 30 min in hot (100 °C) 2·5 N HCl and 10 min in cold 5% HF, rinsed with cold 2·5 N HCl and distilled water five times.

‡ First acid-washed clinopyroxene was pulverized and washed a second time in hot (100 °C) 2·5 N HCl for 30 min.

§ Leachate after first acid wash.

‖ Weight of pyroxene after first acid wash is 98·28% of the weight of pyroxene after H_2O wash. Similarly, the weight of leachate after the first acid wash is 1·72% of the weight of pyroxene after the water wash. Each calculated value is the weighted sum of element concentrations of cpx and leachate after the first acid wash. Measured values are from column 1.

its REE pattern to those of the H_2O-washed and first acid-washed clinopyroxene separates strongly suggests that most of the REE in the leachate are from dissolved clinopyroxene. The large decrease of K, Rb, and Ba contents from the H_2O-washed to the first acid-washed sample is confirmed by the high values of these elements in the leachate, but the leachate is only slightly richer in Sr and Ce. Differences between the calculated and measured concentrations in clinopyroxene (column 5 in Table B1) are very small (0–3%) except for Ce, Rb, and Ba (4·6, 13, and 24%, respectively). A similar observation for a leaching experiment on Ronda peridotites was reported by Zindler *et al.* (1983), and was explained by an uneven distribution of contaminants. Also, the REE concentrations of clinopyroxene after the first and second acid washing are not measurably different.

Silicate glass inclusions were probably still intact after the hot 2·5 N HCl was used in the second acid-washing process without the help of HF. If these silicate glass inclusions represent trapped basaltic magmas, as suggested by Roedder (1965), their contamination effect on the trace element contents of clinopyroxene can be estimated from representative concentrations of trace elements in basaltic liquids and the amount of included glass. To calculate the amount of included glass, it is assumed that K and Rb in clinopyroxene are derived totally from silicate glass inclusions. The proportion of glass inclusions can then be calculated simply by dividing K or Rb contents from clinopyroxene by representative concentrations in basaltic magmas.

Because trace element concentrations for the host alkalic basalt are not available, a calculation involving the first acid-washed clinopyroxene and a prehistoric Hualalai lava [sample 32 of Clague *et al.* (1980*b*)] is used to estimate the extent of the contamination effect. This prehistoric Hualalai lava is chosen because it has the lowest K/Ce and Rb/Ce among the reported Hualalai alkalic basalts, which allows an estimate of the largest contamination effect. The calculation shows that the Ce contamination in all cases is $<0·5\%$ for clinopyroxene from the dunite xenoliths and $<2·5\%$ for clinopyroxene from the wehrlite and clinopyroxenite xenoliths.

However, there is a possibility that the silicate glass inclusions are related to a Hualalai magma other than the host lava. To model such contamination, a Kohala tholeiitic basalt [sample W19 of Feigenson *et al.* (1983)] was chosen because it would produce a contamination greater than any other

analyzed Hawaiian basalt. In this case, the maximum Ce contamination would be 5% for clinopyroxene from the dunite xenoliths and 18% for clinopyroxene from the wehrlite and clinopyroxenite xenoliths.

Because of the extremely high REE contents observed in apatite (for example, up to 1540 ppm Ce; Irving & Frey, 1984), REE concentrations of clinopyroxene would need a significant correction if they contain apatite inclusions. Even though a search with an optical microscope revealed no such inclusions, it is instructive to examine some consequences of assuming that apatite is present in the analyzed clinopyroxenes. Jackson *et al.* (1981) listed whole-rock P_2O_5 concentrations along with modal proportions of clinopyroxene for 17 Kaupulehu ultramafic xenoliths. If all the P_2O_5 is due to apatite inclusions and if apatite inclusions are preferentially concentrated in the clinopyroxene, a positive correlation would exist between P_2O_5 concentration and the modal amount of clinopyroxene. No such correlation exists. Thus, either apatite is preferentially concentrated in other phases or along grain boundaries or it is uniformly distributed throughout. If the abundance of apatite inclusions in clinopyroxene is assumed to be representative of the abundance of apatite inclusions in the xenolith as a whole (the worst case), the effect on REE concentrations can be calculated from the whole-rock P_2O_5 concentrations and representative REE concentrations in apatite. For this calculation, we use 0·01 wt.% P_2O_5 in Kaupulehu dunite xenoliths and 0·02 wt.% P_2O_5 in Kaupulehu wehrlite xenoliths (Jackson *et al.*, 1981) and 1540 ppm Ce in apatite (Irving & Frey, 1984). The maximum contribution of Ce in apatite to the total Ce in dunite clinopyroxene would be 4%. For clinopyroxene-rich xenoliths, the maximum contribution would be 23%. Thus, the REE patterns in Fig. 5 would not be significantly modified. Other mineral inclusions such as mica, if present, would not significantly affect the measured clinopyroxene REE values, because of their much lower REE contents than those of apatite (Irving & Frey, 1984).

From the above arguments, we conclude that grain surface materials contain substantial amounts of K, Rb, and Ba but only minor amounts of Sr and Ce. These surface contaminants are readily removed by leaching. Also, we conclude that contamination from inclusions does not seriously affect the analytical results. Thus, we report the REE and trace element contents of clinopyroxenes obtained after the first acid wash.